

Design and Analysis of Electromagnetic Brake Retarder for HOWO 336 Dump
Truck



Yitagesu Tesfaye Mekuria

**A Thesis submitted to the Department of Mechanical Engineering,
School of Mechanical, Chemical and Materials Engineering**

Presented in partial fulfillment of the requirement for the degree of Master's in
Automotive Engineering

Office of Graduate Studies

Adama Science and Technology University

May, 2024
Adama, Ethiopia

Design and Analysis of Electromagnetic Brake Retarder for Howo 336 Dump
Truck

Yitagesu Tesfaye Mekuria

Advisor: Alemayehu Wakjira Huluka (PhD.)

A Thesis submitted to the department of mechanical engineering,
School of mechanical, chemical and materials engineering

Presented in partial fulfillment of the requirement for the degree of Master's in
Automotive Engineering

Office of Graduate Studies

Adama Science and Technology University

May, 2024

Adama, Ethiopia

DECLARATION

I hereby declare this Master's Thesis entitled "**Design and Analysis of Electromagnetic Brake Retarder for HOWO 336 Dump Truck**" is my own work and has not been submitted for the award of any academic degree, diploma or certificate in any other university. All sources of materials that are used for this thesis have been duly acknowledged through citation.

Yitagesu Tesfaye Mekuria

Name of the student

Signature

Date

RECOMMENDATION

I, the advisor of this thesis, hereby certify that I have read the revised version of the thesis entitled “**Design and Analysis of Electromagnetic Brake Retarder for HOWO 336 Dump Truck**” prepared under my guidance by Yitagesu Tesfaye submitted in partial fulfillment of the requirements for the degree of Master’s of Science in automotive engineering. Therefore, I recommend the submission of revised version of the thesis to the department following the applicable procedure.

Alemayehu Wakjira Huluka (Ph.D.) _____

Major Advisor

Signature

Date

APPROVAL PAGE

I, the advisor of the thesis entitled “**Design and Analysis of Electromagnetic Brake Retarder for HOWO 336 Dump Truck**” and developed by Yitagesu Tesfaye, hereby certify that the recommendation and suggestions made by the board of examiners are appropriately incorporated into the final version of the thesis.

Alemayehu Wakjira Huluka (Ph.D.) _____

Major Advisor

Signature

Date

We, the undersigned, members of the Board of Reviewers of the thesis by Yitagesu Tesfaye have read and evaluated the thesis proposal entitled “**Design and Analysis of Electromagnetic Brake Retarder for HOWO 336 Dump Truck**” and examined the candidate during open defense. This is, therefore, to certify that the thesis is accepted for partial fulfillment of the requirement of the degree of Master of Science in Automotive Engineering.

Chairperson

Signature

Date

Internal Examiner

Signature

Date

Dr. Bisrat Yoseph



20 June 2024

External Examiner

Signature

Date

Final approval and acceptance of the thesis is contingent upon submission of its final copy to the office of postgraduate studies (OPGS) through the department graduate council (DGC) and school dean graduate committee (SGC)

Department head

Signature

Date

School Dean

Signature

Date

Office of Postgraduate Studies, Dean

Signature

Date

ACKNOWLEDGMENT

First and foremost, I would like to thank the Almighty God for His abundant blessings, guidance, and strength throughout the accomplishment of this effort. Secondly, I would like to express my heartfelt gratitude to my family for their constant support and encouragement. I am deeply thankful to Dr. Alemayehu Wakjira for his excellent guidance, advice, and continuous support throughout this process. His experience and suggestions have helped me to shape the project's journey. Furthermore, I want to express deep appreciation to Dr. Ramesh Babu and Dr. Getachew Alemayehu for their time, encouragement, and essential insights. Finally, I want to express my heartfelt gratitude for all who have supported, encouraged, and contributed to this work. Your presence and assistance have been invaluable, and I am extremely thankful for your participation.

DEDICATION

I would like to dedicate this thesis to my dear father, Mr. Tesfaye Mekuria. Your paternal love, care, and support helped me achieve this triumph. You will always have a special place in my heart. May your soul rest in heaven.

Your Loving Son, Yitagesu

TABLE OF CONTENTS

DECLARATION	i
RECOMMENDATION	ii
APPROVAL PAGE	iii
ACKNOWLEDGMENT.....	iv
DEDICATION	v
LIST OF TABLES	ix
LIST OF FIGURES	x
ACRONYMS	xi
NOMENCLATURE	xii
ABSTRACT.....	xiv
CHAPTER ONE	1
INTRODUCTION	1
1.1 Background of the study	1
1.2 Statement of the problem	3
1.3 Objectives.....	4
1.3.1 General Objective	4
1.3.2 Specific objectives	4
1.4 Significance of the study	4
1.5 Scope of the study	5
1.6 Limitations	5
1.7 Organization of Thesis	5
CHAPTER TWO	7
LITERATURE REVIEW	7
2.1 Introduction	7
2.2 Application of Electromagnetic Brake	11
2.3 Types of Electromagnetic Brake Retarder	11
2.4 Components of Electromagnetic Retarder	13
2.4.1 Stator	13
2.4.2 Iron Core.....	14
2.4.3 Coil (winding).....	14
2.4.4 Rotating Disc	14
2.5 Strength and Controlling	14

2.6	Working Principle of Electromagnetic Retarder	15
2.7	Review of Electromagnetic Brake Retarders	16
2.8	Summery of pervious work	20
2.9	Research gap	23
CHAPTER THREE		25
MATERIALS AND METHODS		25
3.1	Materials.....	25
3.1.1	Material selection	25
3.2	Methods.....	27
CHAPTER FOUR.....		30
DESIGN AND ANALYSIS		30
4.1	Introduction	30
4.2	Data and Assumptions.....	30
4.3	Analytical Design of Electromagnetic Brake Retarder	32
4.3.1	Required Braking Force.....	32
4.3.2	Excitation Current.....	34
4.3.3	Design of coil.....	35
4.3.4	Resistance of the wire.....	36
4.3.5	Magnetic field Strength	36
4.3.6	Magnetic flux density	37
4.3.7	Magnetic flux.....	38
4.3.8	Current Density.....	38
4.3.9	Power dissipation, braking torque and force	40
4.3.10	Shaft with spur tooth design	46
4.3.11	Flange Design	48
4.3.12	Bearing Selection.....	49
4.4	CAD Modelling of Electromagnetic Retarder	50
4.4.1	Single Stator and poles	50
4.4.2	Single Rotating Disc model.....	51
4.4.3	Shaft model.....	51
4.4.4	Flange with Internal Gear	51
4.4.5	Assembly 3D modelling	53
CHAPTER FIVE		54

RESULT AND DISCUSSION	54
5.1 Analytical Design Outcome	54
5.2 Static Simulation Outcome	57
5.2.1 Shaft.....	57
5.2.2 Flange	59
5.2.3 Rotating disc	60
5.2.4 Stator with Poles.....	61
CHAPTER SIX.....	63
CONCLUSION AND RECOMMENDATION.....	63
6.1 Conclusion.....	63
6.2 Recommendation and future work	63
6.2.1 Recommendation	63
6.2.2 Future Work Recommendation	64
REFERENCES	65
APPENDIX 1: AWG TABLE	70
APPENDIX 2: SPECIFICATION OF HOWO 336 DUMP TRUCK	71
APPENDIX 3: SPUR TOOTH DESIGN FOR SHAFT	72
APPENDIX 4: PART AND ASSEMBLY DRAWING	73
APPENDIX 5: MATLAB SCRIPT FOR PLOTTING.....	78

LIST OF TABLES

Table 2. 1 Comparison of retarders.....	8
Table 2. 2 Summery of Pervious work	20
Table 3. 1 Materials used for electromagnetic brake retarder	25
Table 3. 2 Properties of copper	26
Table 3. 3 Properties of Alloy Steel.....	26
Table 3. 4 Properties of Aluminium alloy 6061	27
Table 4. 1 Torque Optimization Iteration for Aluminium Alloy 6061	42
Table 4. 2 Torque Optimization Iteration for copper Disc	43
Table 5. 1 Design general results for electromagnetic brake retarder.	54

LIST OF FIGURES

Figure 1. 1 Howo 336 Dump Truck	1
Figure 2. 1 Service Brake System.....	7
Figure 2. 2 Retarder Locations	9
Figure 2. 3 Friction Based Electromagnetic Brake	10
Figure 2. 4 Frictionless Electromagnetic Brake	10
Figure 2. 5 Axial Flux EMR	11
Figure 2. 6 Radial Flux EMR.....	12
Figure 2. 7 Working principle and pole face geometry	15
Figure 2. 8 Schematic diagram of the whole system	16
Figure 3. 1 Methodology.....	29
Figure 4. 1 Schematic diagram of road load equation	32
Figure 4. 2 Response 3D surface for Aluminium alloy 6061	44
Figure 4. 3 Surface response for Copper material	44
Figure 4. 4 Modelled stator and poles.....	50
Figure 4. 5 Rotating disc.....	51
Figure 4. 6 Shaft with spur tooth at both ends	51
Figure 4. 7 Flange 3D model	52
Figure 4. 8 Roller Bearing	52
Figure 4. 9 Assembly of Single stator-rotor of electromagnetic retarder	53
Figure 5. 1 Magnetic Flux Density vs Number of Turns.....	54
Figure 5. 2 Magnetic Flux Density vs Current Relation.....	55
Figure 5. 3 Magnetic Flux Density vs Air gap Relation	55
Figure 5. 4 Magnetic Flux Density vs Braking Torque Relation.....	56
Figure 5. 5 Current vs Braking Torque relation.....	56
Figure 5. 6 Total Deformation and equivalent stress	58
Figure 5. 7 Equivalent strain result	58
Figure 5. 8 Total deformation simulation	59
Figure 5. 9 Equivalent stress and strain result of Flange simulation	59
Figure 5. 10 Total deformation result for rotating disc simulation.....	60
Figure 5. 11 Equivalent strain result of rotating disc simulation.....	60
Figure 5. 12 Equivalent stress result for rotating disc simulation.....	61
Figure 5. 13 Total deformation result	61
Figure 5. 14 Equivalent strain result for stator	62
Figure 5. 15 Equivalent stress simulation result of stator with pole	62

ACRONYMS

AWG	American wire gage
ECB	Eddy Current Brake
ECR	Eddy Current Retarder
EMR	Electromagnetic Retarder
PMR	Permanent Magnet Retarder
FEA	Finite Element Analysis
FEM	Finite Element Method
SL-EMR	Self-excited Liquid Cooled Electromagnetic Retarder

NOMENCLATURE

A_{disc}	Area of rotating disc
a	Addendum (m)
b	Dedendum (m)
C_D	Drag Coefficient
C_{rr}	Coefficient of friction
a_d	Distance between centre of the disc and centre of the pole (m)
A_p	Area of pole face (m^2)
d_{coil}	Coil diameter (m)
F	Force (N)
F_{Air}	Aerodynamic force (N)
F_b	Braking force (N)
F_{net}	Net traction effort (N)
F_{RR}	Rolling Resistance force (N)
$F_{traction}$	Traction force (N)
H	Magnetic field strength (A/m)
i	Current (A)
h_{coil}	Hight/length of the coil (m)
J	Polar moment of inertia (m^4)
J_e	Current density (A/m^2)
L	Length of wire (m)
l_g	Air gap (m)
N	Number of turns
P_d	Power dissipation (watt)

R	Resistance (ohm)
r_{coil}	Coil radius (m)
r_{shaft}	Shaft radius (m)
T	Torque (N-m)
T_b	Braking torque (N-m)
t_{disc}	Thickness of rotating disc
t_{wire}	Thickness of wire (m)
V_{disc}	Volume of rotating disc
W_x	Weight force due to slop (N)
μ_0	Permeability of free space/ air ($\frac{N}{A^2}$)
ρ_c	Resistivity of wire ($\Omega - m$)
σ	Electrical conductivity (Ω/m)
σ_b	Bending stress (Pa)
σ_{tb}	Tooth bending stress (Pa)
τ	Torsional shear stress (Pa)
τ_{solid}	Torsional shear stress for solid shaft (Pa)
τ_{Hollow}	Torsional shear stress for hollow shaft (Pa)
Φ	Magnetic flux (Weber)
ω	Angular velocity (RPM)

ABSTRACT

Now and then braking is utilized by heavy duty vehicles when they are driven at high speed on downhill, or during uphill driving with carrying goods. These frequent braking leads to brake fading in heavy duty vehicles which also causes a serious fatal and material accident. Therefore, adding auxiliary braking system is essential for heavy duty vehicles. Since HOWO 336 dump truck is one of heavy-duty vehicle type and widely used in Ethiopia, it is necessary to add electromagnetic brake retarder feature by systematically studying the required braking torque of the vehicle. Therefore, this study focuses on designing and analysing of electromagnetic brake retarder for the HOWO 336 dump truck. Electromagnetic brake retarders, also known as electric retarders, utilize opposing electromagnetic fields to generate retarding force, providing effective braking without the need for friction. Initially, the required torque for retarding is calculated using the road load equation, assuming the vehicle is driven downhill while carrying goods. A braking force of 38.2 kN is determined, and the corresponding torque on the propeller shaft is 1700Nm. The design of the retarding brake involves determining the necessary current for excitation, considering the number of turns, air gap, and other parameters. The amount of current helps to determine the wire gauge, so that, the total wire length for coil winding was determined. The power dissipation, retarding force and torque were calculated. Optimal torque generation is achieved by adjusting the air gap (0.009-0.0015m), number of turns (800-1000), and current (10-15A). Design expert software generates 19 iterations or combinations. Using the generated iterations, maximum retarding torque was determined by taking aluminium alloy 6061 and copper properties for comparison. Considering the maximum torque generation, the necessary aspects are redesigned. SOLIDWORKS CAD modelling software, ANSYS simulation software are used for modelling and simulation of components of electromagnetic brake retarder. The design process finds an optimal excitation current of 19A and magnetic flux density of 0.1 Tesla. Calculations determined the vehicle's required braking force and torque to be 10 kN and 1700 Nm, respectively. The designed system generated 5 kN of force and 850 Nm of torque, achieving 50% of the required braking capacity and effectively contributing to vehicle braking with reduced power consumption and excitation current.

Keywords: Air gap, Braking force, Coil, Eddy Current, Electromagnet, Retarder

CHAPTER ONE

INTRODUCTION

1.1 Background of the study

Frequent braking is a significant issue in heavy-duty vehicles, particularly when navigating uphill and downhill roads. This constant braking is necessary to control the speed of the vehicle, but it generates a substantial amount of heat due to the friction between the brake pads and rotors. Over time, this excessive heat can lead to brake fade, a condition where the braking effectiveness is significantly reduced. Brake fade poses a severe risk to vehicle safety as it compromises the driver's ability to slow down or stop effectively. This problem is well-documented in heavy-duty vehicles such as dump trucks and buses, which are essential in the construction and transportation industries (Kalaaji & Madi, 2019).

Brake fade is a critical concern for heavy-duty vehicles that frequently travel on varied terrains requiring constant and forceful braking. This issue arises because the friction between the brake pads and rotors produces a significant amount of heat, which can lead to a reduction in braking efficiency. Overheated brakes can become less responsive, increasing the stopping distance and posing a danger to both the vehicle and its surroundings. In industries where safety and operational efficiency are paramount, such as construction and transportation, maintaining effective braking systems is crucial to prevent accidents and ensure the smooth operation of heavy-duty vehicles (Kalaaji & Madi, 2019).



Figure 1. 1 Howo 336 Dump Truck (CNHDT Group, 2023)

Figure 1.1 shows, HOWO 336 dump truck, which is manufactured by Sino Truck in Jinan City, China, is widely available and utilized in Ethiopia. This truck is popular in the construction and transportation sectors due to its robust design and practical features. The HOWO 336 is equipped with an open-box bed that can be hydraulically lifted for easy unloading of materials. Its widespread use in Ethiopia highlights its importance in local industries and underscores the need for effective braking solutions to ensure safety and operational efficiency.

The HOWO 336 dump truck, also nicknamed as "red terror" locally, has gained a notorious reputation due to its involvement in numerous accidents stemming from various causes. A significant issue it faces is its inability to come to a stop efficiently when carrying a full load. Despite the driver's efforts to apply the brakes, the truck's heavy weight and momentum, compounded by brake fade resulting from frequent use, make stopping difficult. This poses serious safety risks for both the driver and other road users. Therefore, it is crucial to address this issue by installing an effective auxiliary braking system or brake retarder. Such enhancements would improve the truck's braking performance, leading to smoother and safer deceleration, and ultimately reducing the likelihood of accidents on the road.

Electromagnetic brake retarders provide a viable solution to the problem of frequent braking in heavy-duty vehicles. Unlike traditional friction-based braking systems, electromagnetic retarders use the principles of electromagnetic induction to generate additional stopping force. This method reduces the reliance on friction, thereby minimizing wear on the braking components. Electromagnetic retarders consist of a stator and a rotor; the stator generates a magnetic field powered by the vehicle's battery, and as the rotor passes through this field, it generates eddy currents. These currents produce an opposing magnetic field that slows down the rotor, and consequently, the vehicle. This system offers a more efficient and reliable way to manage braking in heavy-duty vehicles, enhancing both safety and performance (Zach, 2023).

The braking system is one of the primary systems in any vehicle, playing a crucial role in maintaining control and ensuring safety during driving (Valvolineglobal.com, 2024). In heavy-duty vehicles, the braking system typically comprises a primary braking system and an auxiliary braking system. Brake retarders, which serve as auxiliary braking systems, are particularly important for these vehicles. They help slow down the vehicle in conjunction with the primary service brakes, reducing the strain on the main braking system and preventing overheating and excessive wear. By providing additional braking force, retarders enhance the

overall safety and efficiency of heavy-duty vehicles, which is vital for the protection of goods and passengers (telma.com, 2024).

Electromagnetic brakes have seen increased adoption due to significant technological advancements (Routh et al., 2008). These brakes are now used in a wide range of industries, including aviation, military, healthcare, automation, and transportation. Their broad applicability is due to their efficiency, reduced maintenance costs, and silent operation. In heavy-duty vehicles like the HOWO 336 dump truck, electromagnetic brake retarders offer a significant advantage by providing effective braking without the high wear and heat generation associated with traditional friction-based systems. This makes them an ideal choice for enhancing vehicle safety and reliability.

To integrate an electromagnetic brake retarder on the HOWO 336 dump truck, the first step is to determine the required braking torque. This involves calculating the retarding torque using fundamental magnetic theory. Once the retarding torque is known, the system can be optimized to ensure it provides the necessary braking force. The design process includes creating a CAD model that fits within the available space on the vehicle, considering factors such as the placement of the stator and rotor, and ensuring there is enough room for installation and maintenance. By carefully designing and implementing the electromagnetic brake retarder, the HOWO 336 dump truck can achieve improved braking performance, enhancing safety and operational efficiency.

1.2 Statement of the problem

Due to the frequent and forceful braking required when traveling on uphill or downhill roads, heavy-duty vehicles are particularly exposed to brake fade. On downhill slopes, drivers must continuously or repeatedly apply the brakes to maintain control over the vehicle's speed and prevent excessive acceleration. This repeated braking generates substantial friction, causing the brake disc and pads to overheat. Similarly, although uphill driving generally demands less braking than downhill driving, it still involves frequent brake application to manage speed and navigate corners, contributing to heat build-up. These conditions necessitate the use of auxiliary braking systems to reduce the need for constant braking and mitigate the risk of brake fade. In Ethiopia, the HOWO 336 dump truck is widely used for construction and other purposes, making it essential to equip these vehicles with better retarding systems to prevent accidents caused by brake fade. When HOWO 336 dump truck drivers use the brakes at high speeds, especially when the trucks are loaded, the vehicles can continue to move

uncontrollably, leading to accidents (Addisfortune, 2016; Ethiopian Monitor, 2021). Implementing an efficient retardation system. can significantly reduce these dangers by minimizing brake fade and extending the service life of the vehicle's braking components. Therefore, among types of retarding system, adding electromagnetic brake retarder feature in HOWO 336 dump truck is necessary to avoid frequent braking so that it reduces the occurrence of brake fade. Electromagnetic brake retarders are highly regarded for their silent operation and rapid response times. Their ability to operate quietly ensures minimal noise pollution, contributing to a more comfortable and peaceful driving experience. Moreover, these brake retarders exhibit impressive responsiveness, swiftly engaging and disengaging to provide effective retarding when needed. Earlier versions of electromagnetic brake retarders encountered drawbacks associated with their effect on vehicle mass and power consumption. This stemmed from the significant weight they contributed to the vehicle and the considerable power they consumed, mainly due to their high current usage. Consequently, there arose a critical need to reduce both the mass of the retarder and its power consumption to alleviate strain on the vehicle's power systems.

1.3 Objectives

1.3.1 General Objective

The general objective of this thesis work is to design and analysis of electromagnetic brake retarder for Howo 336 dump truck

1.3.2 Specific objectives

- To systematically analyse required braking torque for electromagnetic brake retarder.
- Analytical design of electromagnetic brake retarder
- Brake Retarding torque optimization at different air gap, current and number of turn combinations.
- Static (stress, strain and total deformation) simulation for components of electromagnetic brake retarder.

1.4 Significance of the study

The following are the significance of implementing electromagnetic brake retarder on HOWO 336 dump truck;

- Minimize repeated braking to reduce brake fading.
- To enhance braking efficiency with the help of the electromagnetic brake retarder

- Extending the life span of Service Brake
- Reducing maintenance cost
- To minimize accidents caused by brake fading of the dump truck

1.5 Scope of the study

The following are scopes of the study of electromagnetic brake retarder for HOWO 336 brake retarder.

- Vehicle: HOWO 336 Dump truck
- Type of auxiliary brake: Frictionless electromagnetic brake retarder
- Design and Analysis: Retarding torque generation
- Software; SOLIDWORKS, ANSYS and design expert.

1.6 Limitations

In order to know the efficiency of the retarding system, prototype and testing the prototype on test work bench are crucial, but construction of prototype and testing the prototype on test workbench needs much money and time. Therefore, the concluded results are limited to theoretical design.

1.7 Organization of Thesis

This thesis work was organized in to 6 chapters; each chapter are detailed as follows;

Chapter 1: Introduction

In this chapter issues that is related to electromagnetic concept are introduced as a background, and also it consists of statement of the problem, general and specific objectives, significance, scope and limitations of the thesis is included.

Chapter 2: Literature Review

Different articles that are previous works of electromagnetic brake retarder was reviewed and their gaps are stated under this chapter. The types of retarders in general was described, and also electromagnetic type in different ways are indicted in this chapter.

Chapter 3: Materials and Methods

Electromagnetic brake retarder has different materials and these materials are stated in this chapter. Methods that are very crucial to meet the formulated objective are indicated also in this chapter.

Chapter 4: Design and Modelling

In this chapter theoretical design details that are the base for electromagnetic retarder was described with formulas and also, the 3D modelling of the system that is drawn using SOLIDWORKS software were presented.

Chapter 5: Result and Discussion

These chapter holds results of mathematical calculations and simulation outputs were imported in this chapter. Additionally, the results that are designed based on different theory and simulation outputs were discussed.

Chapter 6: Conclusion and Recommendation

The final conclusion drawn from the findings are stated with recommendation for future work.

CHAPTER TWO

LITERATURE REVIEW

2.1 Introduction

Braking system is one of the vehicle's seven primary systems, and it is well recognized that it is crucial for maintaining control of the car while driving. The primary braking system and the auxiliary braking system comprises this braking system. As the name implies brake retarder is auxiliary or additional brake system which commonly mounted on heavy duty vehicles. This system has a crucial usage in slowing the vehicle with the help of service brake, that means it cannot completely halt the movement of the vehicle by itself. As shown in figure 2.1, there are mainly two types of service brake which are disk brake and drum brake.

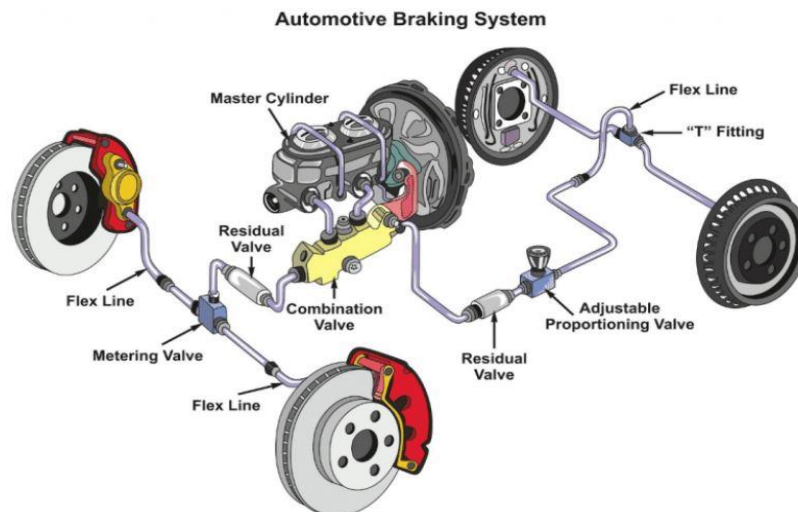


Figure 2. 1 Service Brake System (Bob Rohrman Honda, 2023)

Brake retarders are very helpful for dump truck and bus drivers to keep the safety of the goods they carry and for the safety of passengers as well. There exist several types of brake retarders, such as engine brake retarders, exhaust brake retarders, hydraulic retarders, and electric retarders, that function differently to limit a vehicle's speed (Iyul Nasruddin, 2023).

Electromagnetic brake retarder also called electric retarder, which can be mounted on the driveline, in an axle, or within the transmission. They essentially consist of a stator, or fixed component, mounted to the vehicle's chassis, and a rotor, which is attached to one of the previously stated components. The principles of electromagnetic induction, which effectively use opposing electromagnetic fields to produce extra stopping force, are the basis for all electric

retarders, despite the fact that there are slightly varied variants. The vehicle's battery powers the stator, which generates a magnetic field that the rotor must pass through in order for the system to slow down the car.

Table 2. 1 Comparison of retarders

Aspect/ Feature	Retarder Type			
	Electromagnetic retarder	Hydraulic retarder	Exhaust Brake	Engine Brake
Mechanism	Uses Magnetic induction to generate retarding torque	Uses hydraulic fluid to generate retarding torque	Uses exhaust backpressure to slow the vehicle	Uses engine compression to create resistance
Maintenance	Low: due to fewer moving parts	High: due to hydraulic components	Moderate: affects exhaust system	Requires regular engine maintenance
Heat generation	Generates significant heat	Generates heat	Minimal heat generation	Generates heat internally (in the engine)
Cooling system	Needs cooling system	Needs cooling system	No need (uses engine cooling system)	No need (uses engine cooling system)
Noise	Silent operation	Silent operation	Noisy during operation	Noisy during operation
Response time	Very Fast	Fast: Slower than electromagnetic retarder	Moderate: depends on engine and exhaust configuration	Very fast
Effects on engine operation	No direct impact	No direct impact	Increases backpressure: can affect exhaust flow	Increases engine wear: affects engine cooling
Impact on fuel economy	No significant impact	No significant impact	Can slightly decrease fuel economy due to backpressure	Can slightly decrease fuel economy due to increased engine load

As tabulated in table 2.1, in order to compare electromagnetic brake reader from other types of retarder, aspects like Maintenance, Heat generation, Cooling system, Noise, Response time, Effects on engine operation are Impact on fuel economy are taken (Göhring et al., 2018)(FuelFlowPro.com, 2023). So that taking the trade-off electromagnetic brake retarder makes better.

Eddy currents, or electrical current loops, are produced in the rotor by its movement through the magnetic field, and these loops produce an opposing magnetic field. Any component of the vehicle to which the rotor is attached will slow down as a result of the rotor's magnetic field making it more difficult for it to pass through the stator's opposing magnetic field. This will eventually cause the vehicle to slow down (Zach, 2023). As shown in figure 2.2, electromagnetic brake retarders may have different location according to the design and other parameters like available spaces.

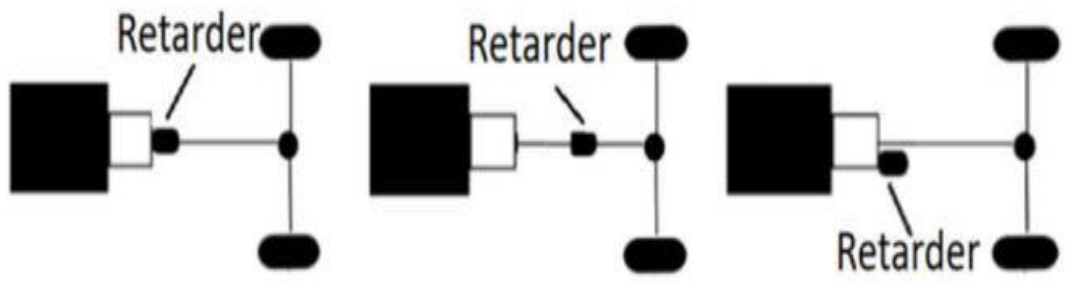


Figure 2. 2 Retarder Locations (Ding et al., 2023)

Because of major technological improvements over the past few decades, electromagnetic brake adoption has increased significantly across a range of industries. These days, industries like aviation, army, automation, healthcare, traction, and even home applications are using these brakes. Experts in these various domains are using electromagnetic brakes more frequently to stop, steady, or precisely control the motion of devices, highlighting the broad applicability and rising need for this cutting-edge technology.

Electromagnetic retarder can be broadly divided in to two, which are friction based and friction less. Figure 2.3 shows, a frictionless electromagnetic brake, a braking system that uses friction in order to slow down or completely stop the motion of a vehicle or piece of machinery is known as a friction-based electromagnetic retarder. Usually, these retarders are made up of revolving discs or drums that are attached to the axle or drivetrain of the car. The retarder

receives an electromagnetic field when braking is applied, which causes the revolving discs or drums to come into contact with stationary parts.

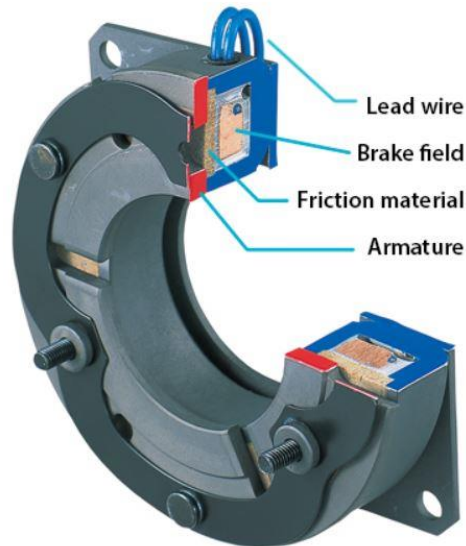


Figure 2. 3 Friction Based Electromagnetic Brake (Electric-brake.com, 2024)

Frictionless electromagnetic retarders function by limiting direct contact between moving parts, which reduces heat production and frictional wear. As shown in figure 2.4, these devices use electromagnetic principles to generate braking force instead of depending on friction. Eddy currents are produced by the interaction of stationary and spinning parts, like permanent magnets and conductive materials, in most cases. Eddy currents and the magnetic field interact to create a braking force that resists the system's motion and enables controlled stopping or deceleration without the need for friction. In systems like energy recovery, industrial machinery, and high-speed trains where reducing wear and heat build-up is essential, frictionless electromagnetic retarders are frequently utilized.

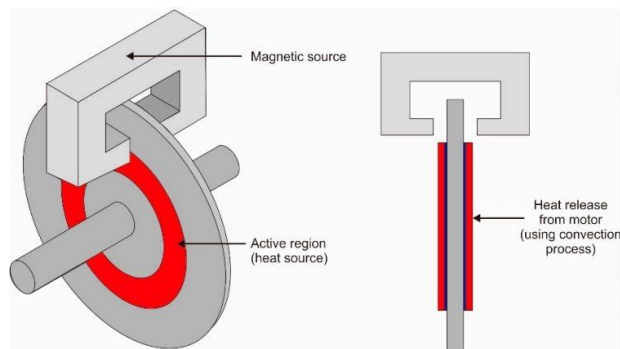


Figure 2. 4 Frictionless Electromagnetic Brake (Putra et al., 2022)

2.2 Application of Electromagnetic Brake

Electromagnetic brake can be used in various sectors of technology such as (Bharti & Anand, 2020); It can be used in Railways to stop or control the speed of trains, in Manufacturing and packaging, in industries to control the motion of products on the conveyer, in Automobile industries to control motion of cars, Medical equipment's and It can be used in robotics.

2.3 Types of Electromagnetic Brake Retarder

Electromagnetic brake retarders can be categorized in to three.

- A. Based on direction of flux
- B. Based on motion of the system.
- C. Based on source of Magnetic Field.

A. Based on direction of flux.

- I. axial flux direction

As shown in Figure 2.5, the magnetic field source of an axial Eddy current brake can be shaped like a disc or as a single unit, but the conductor of the axial version is fashioned like a disk (Waloyo et al., 2019). This axial type, also called the Disc ECB, can use permanent magnets or electromagnets as the generator of the magnetic field. A single disc that is oriented parallel to and facing the conductor serves as the magnetic field source in a single axial ECB arrangement.

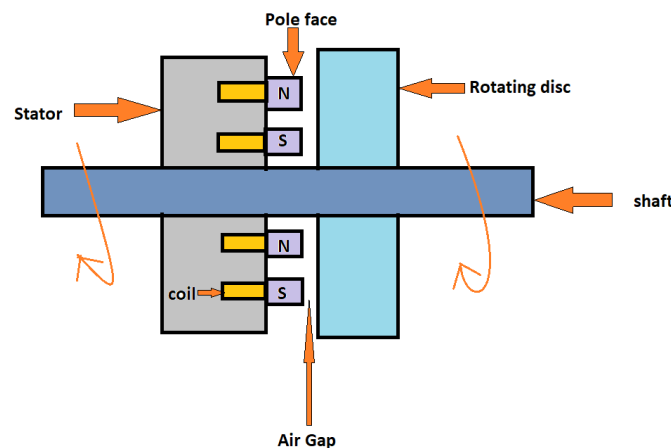


Figure 2. 5 Axial Flux EMR

A dual axial ECB model, with two conductor discs on either side of the magnetic field source, is used to increase energy efficiency. The conductor may capture the total magnetic flux from both poles in this configuration.

II. Radial flux flow

The magnetic flux in this system configuration moves radially outward and toward the rotor's circumference from its centre. Usually, this arrangement consists of a fixed conductor around the source of the rotating magnetic field, which could be a permanent magnet or an electromagnet (J. Wang & Zhu, 2018). As shown in figure 2.6, Eddy currents are created in the conductor as the rotor rotates, which produces a braking force that opposes the motion. Although radial flux eddy current retarders are less prevalent than axial flux designs, they are nonetheless used in a variety of applications where their unique qualities are advantageous, including in some industrial brake systems or dynamometers.

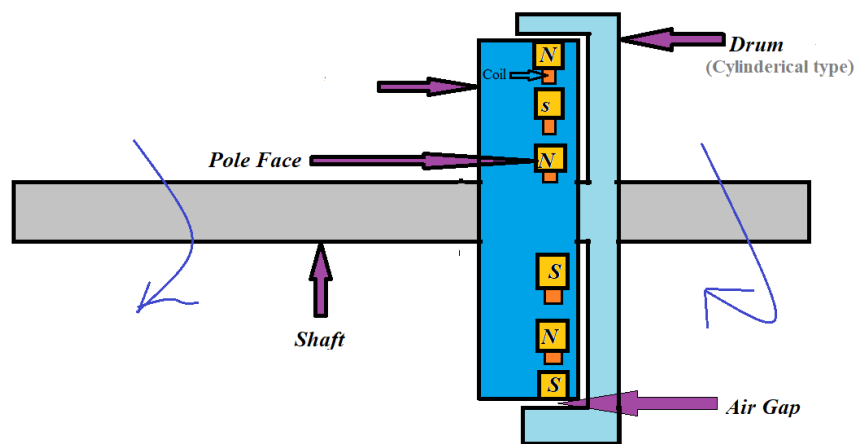


Figure 2. 6 Radial Flux EMR

B. Based on the motion of the system

I. Linear motion EMR

The braking mechanism of linear motion electromagnetic retarders uses electromagnetic principles to slow down or halt linearly moving objects. These systems are widely employed in many different applications where precise control over stopping or deceleration is needed, like industrial machines, roller coasters, and railroads. Usually, a conductive surface and a magnetic field source are positioned along the linear course of motion to form the retarder. The shifting magnetic field causes eddy currents to be created in the conductive surface as the object goes through this configuration, providing a braking force that opposes the motion. By altering the strength of the magnetic field or managing the electrical currents, the braking force can be controlled to accomplish the appropriate level of deceleration or halting (Aravind et al., 2007).

II. Rotational motion EMR

Electromagnetic induction is used in rotational motion eddy current retarders to apply braking force to rotating objects (Kumar Maurya et al., 2011). These systems are frequently used in a variety of settings, including dynamometers, industrial machinery, and car braking systems, when controlled rotational motion braking or acceleration is necessary. Usually, the retarder is made up of a revolving magnetic field source, like an electromagnet or permanent magnet, and a fixed conductor. Eddy currents are created in the conductor as the object spins in the magnetic field's vicinity. These currents produce a braking force that opposes the rotating motion. The required degree of slowing or halting can be achieved by modulating the braking force by varying the strength of the magnetic field or the electrical currents.

C. Based on Source of Magnetic Field

I. Permanent magnet

In this type, Permanent magnets are fastened to a rotating element, like a wheel or shaft, and the conductor is normally positioned stationary in a permanent eddy current retarder. A braking force that resists the motion is created in the stationary conductor when the spinning component passes it due to eddy currents induced by the changing magnetic field (Sakamo et al., 2018)..

II. Electrically produced Magnet

These are temporary magnets made from ferromagnetic cores, like iron or steel, around a coil of wire. The ferromagnetic core of the coil becomes magnetized when an electric current pass through it, creating a magnetic field. By varying the current passing through the coil, the magnetic field's intensity can be adjusted (Lai, 2024).

2.4 Components of Electromagnetic Retarder

Stator, iron core, coil and rotating disc are parts of electromagnetic retarder. They are detailed below;

2.4.1 Stator

The electromagnetic coil-containing fixed portion of the electromagnetic retarder is called stator, it is also a fundamental parts of the axial type eddy current retarder. The individual requirements of the application, such as magnetic performance, efficiency, cost concerns, and operating circumstances, all influence the stator material selection process. Soft iron, silicon steel, and laminated steel (Nategh et al., 2012), are among the most often used materials for stator construction in axial electromagnetic retarders, providing a good balance of magnetic qualities, mechanical strength, and thermal characteristics.

2.4.2 Iron Core

The iron core of the stator assembly functions as a magnetic flux conductor. A magnetic field is produced when current passes through the coils that surround the core. Enhancing the electromagnetic braking system's efficiency is the core's function in concentrating and guiding this magnetic flux. Commonly, ferromagnetic elements like steel or iron are used to make the core. Easily magnetizing and demagnetizing in response to variations in the current passing through the coils is made possible by these materials' high magnetic permeability (Yañez-Valdez et al., 2012).

2.4.3 Coil (winding)

A coil, additionally referred to as the winding or wire coil, creates a magnetic field when an electric current passes through it (Wm. T. Mclyman, 2011). This magnetic field interacts with the rotor, creating braking force and slowing the vehicle. The coil is typically constructed out of insulated copper wire twisted around an iron core. The number of turns and wire gauge can vary depending on the retarder's individual design needs. The coil is connected to an external power source, such as the vehicle's electrical system, using electrical terminals or connectors. When current flows through a coil, it generates a magnetic field in accordance with the right-hand rule, with the path of the magnetic field determined by the current flow.

2.4.4 Rotating Disc

The rotating disc is an essential component of the Retarder, interacting with the magnetic field that surrounds the stator to provide braking force. When electromagnetic coils are energized, they generate a magnetic field that produces eddy currents in the rotating disc. These eddy currents generate a secondary magnetic field that opposes the primary magnetic field, producing braking torque on the disc. Rotating discs are usually made of ferromagnetic materials like iron or steel. These materials are chosen for their capacity to conduct magnetic flux and resist mechanical strains caused by braking. The disc is frequently built with specific features to improve performance, such as fins or grooves to improve heat dissipation and cooling during prolonged braking operations (Smyth & Aiee, 1942).

2.5 Strength and Controlling

Due to gravity and their load, trucks have a constant tendency to accelerate when traveling downhill. As a result, frequent braking and maintaining a safe speed range are essential. ERs are now crucial to breaking the car safely. Brake control is driver-dependent in current ER-based braking systems. ER is activated when the driver wishes to slow down the car. The driver turns off the emergency radio (ER) if the car slows down significantly (Ergün et al., 2014).

2.6 Working Principle of Electromagnetic Retarder

Eddy current retarders use electromagnetic principles to create braking force without requiring physical contact between the braking components (Xuejun et al., 2017). A rotating metallic disk, often made of conductive materials such as copper or aluminium, serves as the heart of this device for generating the braking force. As shown in figure 2.7, the disc is surrounded by either stationary electromagnets or permanent magnets, forming a magnetic field. As the disc spins in this magnetic field, the fluctuating magnetic flux causes electric currents known as eddy currents to flow within the disc. According to Lenz's Law, these eddy currents generate their own magnetic field that opposes the change that caused them. This opposition creates a braking force, reducing the rotation of the disc and, as a result, the vehicle to which it is connected. The kinetic energy of the revolving disc is turned into heat due to the material's resistance to eddy currents, which dissipates as thermal energy into the surrounding environment. Compared to conventional friction-based braking systems, eddy current retarders have advantages such as durability, reliability, and reduced wear, making them particularly ideal for heavy-duty vehicles like trucks and buses.

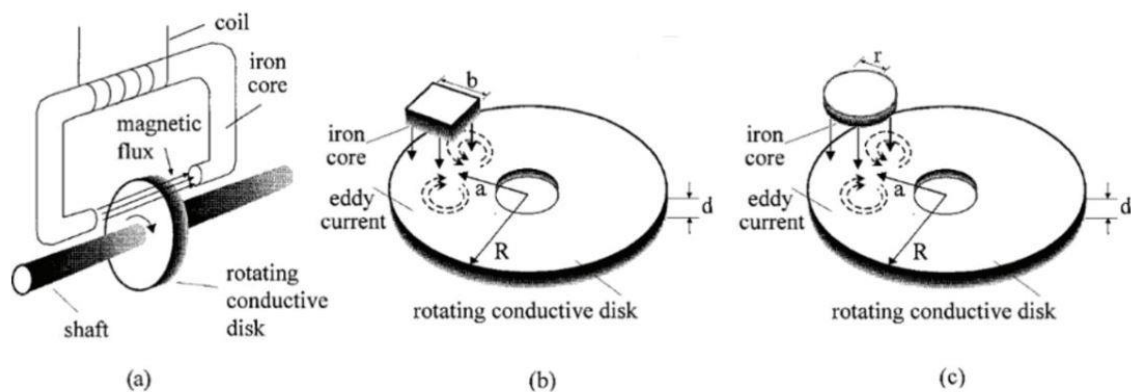


Figure 2. 7 Working principle and pole face geometry (Alexandre J., 2020)

Figure 2.8, shows the general schematic diagram of the system. Electromagnetic brake retarder uses battery as main source of power to generate the retarding torque.

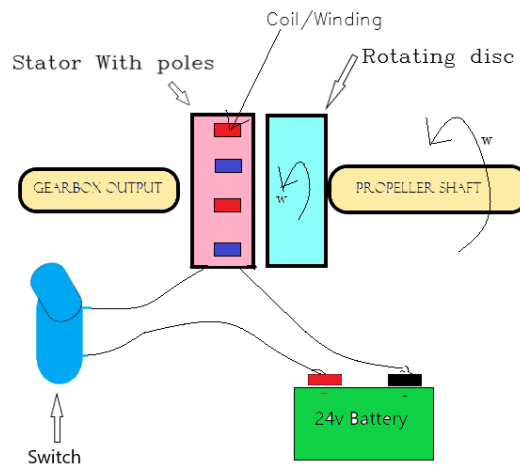


Figure 2. 8 Schematic diagram of the whole system

2.7 Review of Electromagnetic Brake Retarders

Wanyuang Xia et al stated that, two primary drawbacks of the present eddy current retarder are its high energy consumption and overheating risk (Xia et al., 2013). It is battery-operated, which needs 50A, and has a maximum power consumption of 2880W when all eight coils are operating at once. Furthermore, brake failure can be readily caused by the working coil overheating. A self-excited eddy current retarder with reduced energy consumption and enhanced cooling effect has been created to address these problems.

As discussed by Wen Hui and Jiao hi, The TELMA electromagnet retarder was controlled by a manual switch and a pedal micro switch. The proportion of the pedal micro switch that is screwed down determines the brake torque output. Retarder automatically stops working when the bus speed drops below 3 km/h. When the bus reaches 3-5 km/h, the preparation indicator light turns on. The bus can be slowed down with a manual switch or braking pedal (W. H. Wang & Li, 2013)

Kai Zhang et al discussed the numerical analysis and experimentation of a novel self-excited and liquid-cooled eddy current brake (K. Zhang et al., 2014). It includes details about the design, structure, and magnetic circuits of the ECB, as well as the experimental prototype developed based on the analysis. The study focuses on improving braking performance, energy efficiency, and thermal management. It presents mathematical models, analysis of the generator, temperature distributions, and experimental results related to braking characteristics and torque. when the speed was 1500 r/min and the exciting current was 30 A, these results

demonstrate the effectiveness of the proposed self-excited and liquid-cooled eddy current brake in improving braking performance and energy efficiency.

Analytical model and finite element calculation of the electromagnetic retarder's braking torque (Ye et al., 2014). The flux tube and armature reaction approach are used in this research to propose an analytical model that predicts the braking torque of an electromagnetic retarder. It also creates model for the electromagnetic retarder in two and three dimensions using finite elements. Results from the 2-D finite element model are in good agreement with the air-gap flux density computed by the analytical method. Furthermore, when the speed is less than 1250 r/min, the computed braking torque from the 3-D model shows just a 10% inaccuracy in comparison to the measured torque.

An in-depth analytical model for three-dimensional axial-flux eddy-current couplings and brakes was presented by Thierry Lubin and Abderrezak Rezzoug. It provides precise torque and axial force formulas that are relevant to steady-state circumstances (regular speed operation). The moving conducting component's response field caused by induced currents is included in the model. In order to simplify the study, the researchers solve the problem in 3-D Cartesian coordinates, ignoring curvature effects, by assuming that linearization occurs at the mean radius (Lubin & Rezzoug, 2015).

Reza Y. and Mojtaba M. presents a new electromagnetic brake design and its analysis (Yazdanpanah & Mirsalim, 2015). It details the brake system components and their functions, including the electrical model. Numerical optimization focuses on key components like the ECB and RB for improved performance. Prototyping and validation through simulations and experiments ensure functionality across various conditions. A closed-loop speed control scheme evaluates the brake's control capabilities.

Kai Zhang et al conduct a comprehensive analysis of the SL-EMR braking system through various simulations and bench test (K. Zhang et al., 2015). They evaluate generator parameters, braking performance, thermal field, and the electromagnetic field model using the finite-element technique (FEM). The findings support the system's dependability by showing a 6% difference between FEM calculations and experimental data. In addition, it is shown that the integrated generator has the capability to supply the brake system with exciting current. The braking torque decreases moderately (10.4%) when the system is continuously braking, demonstrating the system's resilience.

Zhou Q. et al. work indicate that, Parameter Analysis for the Eddy Current Brake with Construction of a Model, Simulation, and Sensitive Analysis for torque Stabilization (Zhou et al., 2015). The article introduces the idea of antimagnetic force by drawing on the magnetic circle theory. Employing the created ECB model, it runs simulations to examine the features of braking torque. The elements impacting torque production properties are studied by an adjustment of the structural design parameters of the ECB. A nominal maximum braking torque of an ECB has been shown to be optimized by adjusting internal parameters. Next in importance to the maximum braking torque are the rotor disc and air-gap thickness, then the radius of the pole shoe's cross-section area and its distance from the rotating centre.

In Yasa et al article, flux linkage and induced magnetic force are analysed using FEA software to develop analytical models for evaluating the time-domain electrical performance of electromagnetic brakes (Yasa et al., 2016). Furthermore, using 3D FEA software, it develops a thermal model for EM brakes and analyses their thermal behaviour. Performance criteria and parameters are properly balanced by the development of an optimization algorithm. High heat conductivity epoxy resins should be used to fill the housing, and materials with higher magnetic saturation capacity should be chosen for the armature and housing. It has been observed that elevated coil temperatures reduce friction and magnetic flux, which in turn reduces torque capacity.

By Hu D. et al., the electromagnetic brake on a passenger car was optimally designed and controlled to save energy (Hu et al., 2019). In this article, prediction models for an electromagnetic brake's power usage and braking efficiency was introduced. A simulation platform that uses hardware-in-the-loop is used to validate these models. The electromagnetic brake was made with the express purpose of using less energy. Furthermore, a technique for managing energy conservation in the electromagnetic brake was suggested.

Jin et al. introduces a thermal examination of a hybrid excitation linear eddy current brake (Jin et al., 2019). This brake type generates its air gap flux using both excitation windings and permanent magnets, resulting in a significant and modifiable braking force. However, the excitation windings and conductor plate can experience substantial heating, potentially leading to a decline in braking performance or device damage. To address this concern, the paper outlines the brake's structure and operational principle, develops an analytical model, and constructs a thermal network model that integrates real air flow conditions. Finally, the paper

validates the thermal network model through steady and dynamic thermal experimental measurements.

The Permanent Magnet Retarder, designed for heavy vehicles employs eddy-current braking principles and features with adjustable braking torque (Ye, Cao, et al., 2019). The performance was analysed using a multi-physics field coupling model encompassing electromagnetic, thermal, and fluid dynamics. A new method was proposed to predict permanent magnet demagnetization, considering dynamic air-gap flux density and temperature effects.

Lezhi Ye et al, focused on testing and optimization of a liquid-cooled, twin air-gap eddy current retarder (ECR) for heavy vehicle auxiliary braking. The suggested ECR seeks to address problems with conventional ECRs' excessive rotor weight and heat fading during continuous braking (Ye, Liu, et al., 2019).

An electromagnetic braking system uses both magnetic force and electricity to halt motion of the vehicle. The magnetic force produced by the applied voltage or current draws in the brakes, further stopping the vehicle's rotatory motion. While there are other disc designs that work similarly to single friction surface brakes, the majority of electromagnetic brakes use a single friction surface. The hub, armature, and field coil make up its main components (Bharti & Anand, 2020).

Rui-Jan published Structure design and coordinated control of electromagnetic and frictional braking system based on a hub motor (R. J. Zhang, 2021). This article explores the assessment of braking performance within an integrated system. It introduces a unique combination of electromagnetic and frictional braking systems through a novel composite structural design. Mathematical and simulation models are developed to evaluate the braking capabilities of this integrated setup. Additionally, a fuzzy controller implemented using MATLAB/Simulink is crafted to authenticate and analyse the operational efficiency of the integrated system.

Karade et al mentioned that a minor leak in an oil or air braking system might cause the brakes to fail completely in-service brakes. But four-disc plates, coils, and firing circuits are independently attached on each wheel in an electromagnetic braking system, even if one coil fails, the brake does not fail completely because the remaining three coils work properly. (Karade et al., 2022).

2.8 Summery of pervious work

The following table 2.2 shows, the author, methodology followed, findings and limitation or their gap.

Table 2. 2 Summery of Pervious work

Autor	Title	Methodology	Finding	Limitation/gap
(Xia et al., 2013)	Experiment study and design of self-excited eddy current retarder	<ul style="list-style-type: none"> ✓ Mathematical modelling and MATLAB/Simulink ✓ Small scale modelling (150 times smaller) for testing 	<ul style="list-style-type: none"> ✓ Power generation for self-excitation 	<ul style="list-style-type: none"> ✓ Higher mass and cost due to addition of generator. ✓ High excitation current (50A) ✓ Material type not mentioned
(W. H. Wang & Li, 2013)	Study on matching electromagnet retarder for city bus with force analysis based on brake directional stability	<ul style="list-style-type: none"> ✓ Force analysis 	<ul style="list-style-type: none"> ✓ Directional stability was analyzed with operation of electromagnet alone at dry, rainy and snow weather conditions. 	<ul style="list-style-type: none"> ✓ The retarder studied has mass of 101 kg ✓ High excitation current (49A) ✓ Material type not mentioned
(K. Zhang et al., 2014)	Numerical analysis and experimentation of a novel self-excited and liquid-cooled eddy current retarder	<ul style="list-style-type: none"> ✓ 3D FEA using J-MAG and ANSYS software ✓ Brake power generation testing 	<ul style="list-style-type: none"> ✓ Power generation. ✓ Water cooling mechanism. 	<ul style="list-style-type: none"> ✓ Torque generation performance not mentioned. ✓ Higher excitation current (30A) ✓ Higher mass due to addition of generator. ✓ Material type not mentioned
(Ye et al., 2014)	Analytical model and finite element computation of braking torque in electromagnetic retarder	<ul style="list-style-type: none"> ✓ Flux tube and armature reaction method for analyzing braking torque. ✓ FEA using JMAG software ✓ Comparison 	<ul style="list-style-type: none"> ✓ 10 error in comparison of analytical model and FEA model 	<ul style="list-style-type: none"> ✓ Material for rotating disc is not mentioned. ✓ Maximum excitation current is 26A ✓ 1.9T magnetic flux

				density was registered which indicates higher current
(Lubin & Rezzoug, 2015)	3-D Analytical Model for Axial-Flux Eddy-Current Couplings and Brakes under Steady-State Conditions	<ul style="list-style-type: none"> ✓ FEA for axial flux eddy current using COSMOL Multiphysics® software. ✓ Maxwell stress tensor method for determining torque and axial force 	<ul style="list-style-type: none"> ✓ The torque and the axial force formulas have been obtained from the Maxwell stress tensor method. ✓ Determination of torque-speed characteristics. 	<ul style="list-style-type: none"> ✓ Cooling mechanism not mentioned ✓ Excitation current is not indicated
(Yazdanpanah & Mirsalim, 2015)	Hybrid Electromagnetic Brakes: Design and Performance Evaluation	<ul style="list-style-type: none"> ✓ FEA ✓ Prototyping ✓ Validation 	<ul style="list-style-type: none"> ✓ Power generation using regenerative braking. 	<ul style="list-style-type: none"> ✓ Excitation current not mentioned ✓ Cooling system is not identified ✓ Material type for conducting disc is not mentioned.
(K. Zhang et al., 2015)	Design and performance of a self-excited and liquid-cooled electromagnetic retarder	<ul style="list-style-type: none"> ✓ FEM is used to determine the characteristics of generator ✓ Performance test 	<ul style="list-style-type: none"> ✓ Power generation using brushless generator ✓ Liquid cooled retarder was designed 	<ul style="list-style-type: none"> ✓ Higher current used (30A)
(Zhou et al., 2015)	Parameter Analysis on Torque Stabilization for the Eddy Current Brake: A Developed Model, Simulation, and Sensitive Analysis	<ul style="list-style-type: none"> ✓ Mathematical modelling ✓ Simulation using MATLAB/simulation 	<ul style="list-style-type: none"> ✓ Studied the effect of air gap and pole face cross-sectional area. 	<ul style="list-style-type: none"> ✓ Cooling system not mentioned ✓ Wire thickness and its length is not stated

(Yasa et al., 2016)	A multidisciplinary design approach for electromagnetic brakes	<ul style="list-style-type: none"> ✓ Analytical model is derived ✓ FEA is performed ✓ Testing 	<ul style="list-style-type: none"> ✓ Material is selected and Braking torque is calculated ✓ Good agreement of results with testing. 	<ul style="list-style-type: none"> ✓ Frictional electromagnetic brake is used. ✓ Location of the retarder is not mentioned ✓ Cooling system is not clearly stated.
(Hu et al., 2019)	Energy saving optimal design and control of electromagnetic brake on passenger car	<ul style="list-style-type: none"> ✓ Analytical design ✓ Simulation ✓ Testing 	<ul style="list-style-type: none"> ✓ Influence of nonlinear materials are presented. 	<ul style="list-style-type: none"> ✓ Energy saving optimal design by changing number of poles is necessary.
(Jin et al., 2019)	thermal Analysis of a Hybrid Excitation Linear Eddy Current	<ul style="list-style-type: none"> ✓ Structure and working principle were described ✓ Analytical model was built ✓ Testing the model using CFD ✓ FEA 	<ul style="list-style-type: none"> ✓ Influence of temperature rise on the braking torque generation is analyzed. ✓ Thermal network model is suggested for eddy current thermal management 	<ul style="list-style-type: none"> ✓ Rotational eddy current brake thermal management is not mentioned.
(Ye, Cao, et al., 2019)	Multi-Field Coupling Analysis and Demagnetization Experiment of Permanent Magnet Retarder for Heavy Vehicles	<ul style="list-style-type: none"> ✓ FEA ✓ Testing torque and temperature rise on bench 	<ul style="list-style-type: none"> ✓ Braking torque generation using permanent magnet ✓ The braking distance is shortened 34% 	<ul style="list-style-type: none"> ✓ Retarder stops if permanent magnet fails.
(Ye, Liu, et al., 2019)	Optimization design and test of dual air-gaps and liquid-	<ul style="list-style-type: none"> ✓ FEA ✓ Kriging approximation method used for optimization 	<ul style="list-style-type: none"> ✓ Braking torque using permanent and eddy current braking 	<ul style="list-style-type: none"> ✓ Combining the two types of magnet leads to higher mass

	cooled eddy current retarder		<ul style="list-style-type: none"> ✓ Added liquid cooling system. ✓ Heat fade ratio becomes 13% 	and complexity
(Bharti & Anand, 2020).	Introduction to Electromagnetic Braking System	<ul style="list-style-type: none"> ✓ Theoretical background 	<ul style="list-style-type: none"> ✓ Electrically controlled Frictional electromagnetic brake system is studied. 	<ul style="list-style-type: none"> ✓ There is no clear methodology ✓ Cooling system not mentioned
(R. J. Zhang, 2021)	Structure design and coordinated control of electromagnetic and frictional braking system based on a hub motor	<ul style="list-style-type: none"> ✓ Mathematical modelling ✓ Simulation using MATLAB/ Simulink 	<ul style="list-style-type: none"> ✓ Retarding using electromagnetic and frictional braking system. 	<ul style="list-style-type: none"> ✓ Wear ✓ Additional cost for maintenance ✓ Cooling system is a key issue in this article
(Karade et al., 2022).	Electromagnetic Braking System	<ul style="list-style-type: none"> ✓ Theoretical background of service brake and electromagnetic brake system is presented 	<ul style="list-style-type: none"> ✓ Identifying advantages and disadvantages of electromagnetic brake retarder. ✓ Factors that affect electromagnetic brake torque generation are listed. 	<ul style="list-style-type: none"> ✓ Mathematical model and any simulation are not mentioned ✓ There is no clear formula for braking torque generation.

2.9 Research gap

The available research on eddy current and electromagnetic braking systems offers significant insights into electromagnetic brake retarders. These systems have advanced considerably, enhancing their performance and application across various sectors. Despite this progress, there remains a notable gap in research, particularly concerning the effects of using high current levels (Xia et al., 2013)(Alexandre J., 2020). Higher current levels are directly linked to

increased power consumption, presenting design and efficiency challenges for electromagnetic retarders. Studies indicate that the current required to activate these retarders typically falls between 30A and 50A. Although effective for certain uses, this range does not fully explore the potential and limitations of employing even higher currents.

Another significant gap in the research involves the use of higher magnetic flux densities. The maximum magnetic flux density reported in existing studies is around 1.95 Tesla. Achieving such high flux densities necessitates higher current because the magnetic field strength is directly proportional to the current in the electromagnet coils. Therefore, stronger magnetic fields require more current, leading to several practical issues. One primary concern with higher current consumption is the need for thicker wires to handle the increased current without overheating or failing. These thicker wires require more space when wound around the electromagnet's core material, complicating the design and potentially reducing the efficiency of the electromagnetic brake retarder. Moreover, using thicker wires and higher currents can increase material costs and may require more complex cooling systems to manage the additional heat generated. This complexity poses further challenges in the practical implementation and broader adoption of high-current electromagnetic braking systems.

The previous electromagnetic brake retarding system utilized a double rotor disc configuration with 16 poles. By simplifying the system to a single rotor disc with 8 poles, it is possible to significantly reduce the amount of current needed for operation. This reduction in current directly translates to lower overall power consumption, additionally by simplifying the retarding system also minimizes the weight of electromagnetic retarders hence it can reduce inertia and fuel consumption due to addition of the retarding system on the vehicle.

CHAPTER THREE

MATERIALS AND METHODS

3.1 Materials

In this section, basic components of the electromagnetic system are listed below and, selection of material which are necessary for design and analysis of the system is described in this section. Table 3.1 shows materials that are used for this research work.

Table 3. 1 Materials used for electromagnetic brake retarder

No.	Material	Description
1.	Coil wire	For generation of magnetic field
2.	Electromagnet Core	To wind the wire on it
3.	Stator	Fixed material used to hold other components
4.	Rotating disc	For generation of eddy current
5.	Shaft	To Transmit power
6.	Flange	To connect gearbox with retarder and propeller shaft
7.	Bearing	To support rotating part
8.	Computer	For design, modeling and documentation.
9.	Software; SOLIDWORKS, ANSYS, Design Expert.	For design, simulation and Optimization

3.1.1 Material selection

Since material selection is the process of choosing the most suitable material for the desired application, for this case, for electromagnetic retarder, materials which are necessary for design is selected in this section.

A. Electromagnet Core: it is a critical component that increases the magnetic field produced by the coil. It collects and directs the magnetic flux generated by the electricity flowing through the coil. Materials with high magnetic permeability, such as iron, nickel, and cobalt, are typically utilized for electromagnet cores because they effectively concentrate magnetic flux. Soft iron has become particularly popular because it is inexpensive and easily magnetized and demagnetized (Grandi et al., 2004). Therefore, iron is selected for electromagnetic core.

B. Material for Coil wire: Copper is one of the most popular coil wire materials due to its greater electrical conductivity, thermal conductivity, and corrosion resistance. It is widely utilized in applications requiring great electrical efficiency, such as transformers, motors, and inductors(Sari et al., 2020). Therefore, coil is selected for winding and generation of magnetic field and the electrical properties of copper is tabulated on Table 3.2.

Table 3. 2 Properties of copper (Azom.com, 2024b)

Copper	
Properties	Value
Density (kg/m^3)	8940
Maximum Tensile Strength (MPa)	390
Electrical conductivity (Siemens/m)	5.96×10^7
Electrical Resistivity (ohm-m)	1.68×10^{-08}

C. Material for Stator, Shaft, Flange and Bearing: Alloy steel is a form of steel that incorporates alloying elements in addition to carbon, which is found in conventional carbon steel. Manganese, silicon, chromium, nickel, molybdenum, vanadium, and other elements are examples of alloying elements. These components improve the steel's many qualities, including strength, hardness, toughness, corrosion resistance, and wear resistance. Alloy steels are widely employed in a variety of industrial applications that require specialized qualities, including automobile parts, machinery components, tools, pipelines, and structural elements(Xometry.com, 2024). Therefore, alloy steel is used for design of Stator, shaft, flange and bearing. The properties of alloy steel are tabulated on table 3.3.

Table 3. 3 Properties of Alloy Steel(Azom.com, 2024a)

Alloy Steel	
Properties	Value
Density (kg/m^3)	7850
Maximum Tensile Strength (MPa)	620
Hardness, Vickers (--)	217
Hardness, Rockwell C (--)	15

D. **Rotating Disc:** The rotating disk in an eddy current retarder system generates braking force through the interaction of the magnetic field and induced eddy currents. Aluminium alloy, AL6061 is taken for rotating disc of electromagnetic brake retarder because, it has higher electrical conductivity (Baharom et al., 2012), it is better at producing eddy current (Sailesh & Krishna, 2021) and it is less cost and minimum density (Mupona & Singh Tomar, 2013) compared to the zinc and nickel materials. Therefore, aluminium is used for rotating disc design. Table 3.4 shows the properties of aluminium alloy 6061.

Table 3. 4 Properties of Aluminium alloy 6061 (Ashby, 1999)

Aluminum Alloy 6061	
Properties	Value
Density (kg/m^3)	2700
Maximum Tensile Strength (<i>MPa</i>)	276
Electrical conductivity (<i>Siemens/m</i>)	2.459×10^7
Electrical Resistivity (ohm-m)	4.066×10^{-08}

3.2 Methods

In order to meet the formulated general and specific objective of these thesis work, the following methodology was taken in to account;

- ❖ **Literature Review:** literature review is done out on electromagnetic brake retarder to identify design parameters and research gaps.
- ❖ **Data collection and assumptions:** information of HOWO 336 Dump truck which is directly related to the electromagnetic retarder just like, engine maximum torque, maximum angular speed, gear ratio etc. are collected, and also the data that are not available directly are assumed reasonably.
- ❖ **Designing and 3D modelling:** For the design of electromagnetic retarder system fundamental mechanical and electrical theories and formulas are used. In the case of 3D modelling of the electromagnetic components, SOLIDWORKS (Computer aided design) software is used. The following general steps are applied for part and assembly drawings;

- A. Open SOLIDWORKS Software; so that new blank document launches
 - B. Choose parts for part drawing the components; and choose assembly for assembling the part drawing.
 - C. Sketching and Adding Dimensions and Relations
 - D. Extruding and Revolving: after completing sketching extruding, revolving etc. can be used to get 3D geometry.
 - E. Apply the desired feature: fillet, chamfer, hole, shell, etc., can be used to customize 3D models.
- ❖ **Optimization of retarding torque:** Design expert software can be used to determine the iteration or combinations of air gap, current and number of turns, and using torque formula, the calculation is done by hand and tabulate for corresponding result, then determine the optimum value
- ❖ **Static Simulation of components;** using ANSYS simulation software, the static structural analysis, i.e. total deformation, equivalent stress strain analysis is simulated. The following steps are necessary to simulate on ANSYS simulation software.
- A. Launch ANSYS Workbench.
 - B. Initiate a New Static Structural Analysis.
 - C. Import or Generate the Geometry. Specify the Material Properties.
 - D. Set the Mesh Size and Generate the Mesh.
 - E. Establish Boundary Conditions: add Fixed Supports or other relevant supports.
 - F. Apply Loads: apply design-specific loads such as Forces, Torques, Pressure, or other types.
 - G. Solve the Model.
 - H. Perform Post-Processing
 - I. Obtain Results for Total Deformation, Equivalent (von Mises) Stress, and Equivalent Strain.

Figure 3.1 shows the methodology followed to design and analysis of electromagnetic brake retarder for Howo 336 dump truck.

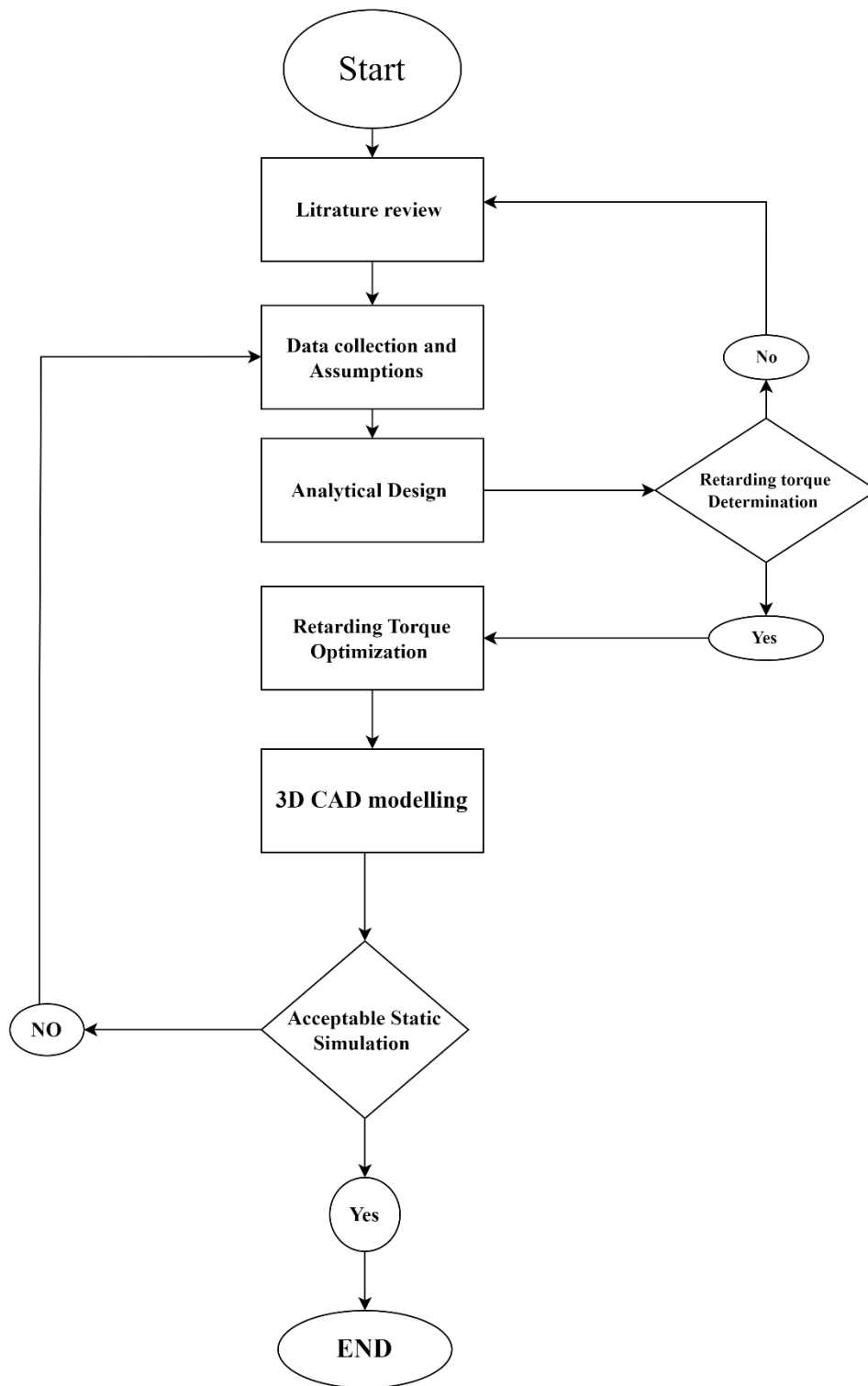


Figure 3. 1 Methodology

CHAPTER FOUR

DESIGN AND ANALYSIS

4.1 Introduction

To gain a comprehensive understanding of the electromagnetic retarder and its operational dynamics, it's crucial to combine theoretical study with practical insights obtained from industry visits. Hence, visits to facilities such as common Sinotruck garage in Adama were undertaken to gather first-hand information and assess the space available for the installation of the electromagnetic retarder. Following the visit, it was determined that the most suitable location for the retarder would be between the gear box output and propeller shaft input flanges, connected via a shaft. Additionally, the Anbesa garage in Addis Ababa provided valuable insights into the functionality of the system, particularly in the context of buses. Using this in mind, the design and analysis process is done by utilizing assumptions, data and fundamental theories with their calculations.

4.2 Data and Assumptions

The following data and assumptions are taken in to consideration for design and modelling of the retarding system.

- ✓ Maximum Full load mass of the vehicle = 25,000kg (see appendix 2): To systematically determine the required retarding torque, knowing the vehicle's full load mass is crucial.
- ✓ Maximum Engine torque of the vehicle = 1350N-m @1100-1600 rpm (see appendix 2):
- ✓ Final Drive ratio=5.73 (see appendix 2.): this parameter is also very important to determine the required retarding torque i.e. it is used in the road load equation for traction force determination.
- ✓ Take Maximum angular speed = 1600 RPM =167.55 RPS: angular speed is needed in the determination of required retarding torque for the vehicle and in the generation of retarding torque by eddy current generation.
- ✓ Radius of vehicle wheel = 0.245m (see appendix 2.): wheel radius is used to calculate the torque available on the wheel using road load equation.
- ✓ Assumed Source of power is a battery having 24 v: in order to excite the electromagnetic brake retarder 24v battery is used as source of power.
- ✓ Assumed thickness of rotating disc and Air gap are 12mm and 1mm respectively: Thicker discs can accommodate a greater number of eddy currents, which are loops of electric current generated within the conductor by a varying magnetic field. This

enhances the overall retarding torque. The air gap size influences the reluctance (resistance to magnetic flux) within the magnetic circuit. A smaller air gap decreases reluctance, resulting in a stronger magnetic field for the same amount of current (Putra et al., 2021).

- ✓ Diameter of the disc=0.34m=340mm: rotating disc plays the main role in generation of eddy current.
- ✓ Material selected for Rotating disc = Aluminium Alloy=Al6061(see chapter 3)
- ✓ Material selected for wire = copper (see chapter 3)
- ✓ Material selected for core = iron (see chapter 3)
- ✓ Material selected for remaining components = steel alloys (see chapter 3)
- ✓ Assumed Coefficient of friction=0.020: this coefficient of friction is taken for normal asphalt or gravel roads(Atamnia et al., 2021) and it is essential in calculating rolling resistance.
- ✓ width and height of the vehicle=2.5m*3.4m: (see appendix 2). In order to perform aerodynamic force of the vehicle the width and height of the vehicle is important that is to determine the area of the front facing of the vehicle to air.
- ✓ Assumed Coefficient of drag (CD) value for heavy duty vehicles=Drag Coefficient=0.8 CD value for heavy duty vehicles ranges from 0.6-0.8 (Chowdhury et al., 2019) so that 0.8 is taken for calculation of aerodynamic resistance.
- ✓ Assumed Number of poles =8: poles are very necessary to hold the coil (to wind the wire on it) to generate magnetic induction.
- ✓ Assumed total winding number of turns = 400: number of turns are essential in determining the length of the wire, magnetic strength and magnetic flux densities in general.
- ✓ Density of air=1.225 kg/m³.
- ✓ Assumed pole diameter=0.05m=50mm
- ✓ Assumed diameter of coil without iron core =0.02m
- ✓ Assumed vehicle Speed=80km/Hr = 22.22m/sec
- ✓ Assumed the height of the coil = 0.10m
- ✓ Slop = 7 degree downhill (lima limo Road grade is 12% which is around 7 degree)
- ✓ resistivity of the wire (i.e. copper = $1.72 \times 10^{-8} \Omega\text{-m}$)
- ✓ permeability of air= $4\pi \times 10^{-7} \text{ N/A}^2$

4.3 Analytical Design of Electromagnetic Brake Retarder

4.3.1 Required Braking Force

The road load equation is a mathematical equation utilized to depict the forces exerted on a vehicle as it travels at a consistent speed along a road. These forces predominantly consist of aerodynamic drag, rolling resistance, and gravitational forces. By employing this equation, the energy required to halt the vehicle can be determined so that, the vehicle can be controlled (thecartech.com, 2024).

So that, from the relation of road load equation;

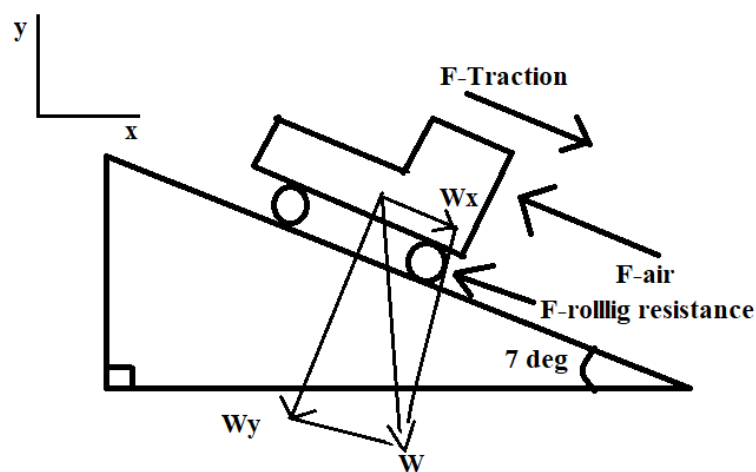


Figure 4. 1 Schematic diagram of road load equation

Figure 4.1, shows the schematic diagram of the road load equation, which gives the following general equation for net traction effort

$$F_{net} = F_{traction} + W_x - F_{RR} - F_{Air}$$

Where;

A. $F_{traction} = \text{Traction force} = \frac{\text{Wheel torque}}{\text{wheel radius}}$

Therefore, substituting the data for wheel torque and wheel radius traction force gives;

$$F_{traction} = \frac{1350Nm * 1 * 5.73}{2 * 0.254m} = 15,227.36 N$$

B. $W_x = \text{Weight force due to slop} = \text{mass} * \text{gravity} * \sin\theta = mg\sin\theta$; therefore, using 7-degree slop downhill and substituting the values for mass and gravity gives;

$$W_x = 25000kg * 9.81 \frac{m}{s^2} * \sin 7^\circ = 29,888.45 N$$

C. $F_{RR} = \text{Rolling Resistance force}$; Rolling resistance of the vehicle can be calculated as follows;

$$F_{RR} = \text{mass} * \text{gravity} * \cos\theta * \text{coefficient of friction} = m * g * \cos\theta * C_{rr}$$

Therefore, substituting for mass, gravity and cosine of 7 degree; rolling resistance gives;

$$F_{RR} = m * g * \cos\theta * C_{rr} = 25,000kg * 9.81 \frac{m}{s^2} * \cos 7^\circ * 0.020 = 4868.44 N$$

$$D. F_{Air} = \text{Aerodynamic force} = \frac{1}{2} * \rho_A * C_D * V^2 * A_f$$

Where; $\rho_A = \text{density of air} = 1.225 \frac{kg}{m^3}$, $A_f = \text{front area} = \text{width} * \text{height} = 2.5m * 3.4m = 8.5m^2$ and $C_D = \text{Drag Coefficient} = 0.8$; therefore substituting the values into Aerodynamic force formula, it gives the following results;

$$F_{Air} = \frac{1}{2} * 1.225 \frac{kg}{m^3} * 8.5m^2 * 22.22^2 * 0.8 = 2056.4 N$$

Since; traction effort, weight due to slope of the road which is in the direction of traction effort, rolling resistance and aerodynamic resistance are calculated on the above; net force becomes;

$$F_{net} = 15227.36N + 29,888.45N - 4868.44N - 2056.4N = 28,278.06 N = 38.2 kN$$

Therefore, 38.2 kN is the net traction force calculated for wheels, but to get braking torque available on the wheel can be determined using following formula;

Since the wheel radius of the vehicle is 0.254m,

$$T_{wnet} = F_{wnet} * r_w = 38200N * 0.254m = 9702.8 Nm$$

Therefore, the braking torque available propeller shaft can be calculated by dividing the final driving ratio and gear ratio, therefore;

$$T_{pro} = \frac{9702.8Nm}{1 * 5.73} = 1693.33 \text{ say } 1700Nm$$

Then, the braking force available on the rotating disc which is connected with propeller shaft via flange, can be determined by using the radius of the rotating disc of the retarder, then;

$$F_{pro} = \frac{1700Nm}{0.0825m} = 10000N = 10kN$$

Dividing the braking Force available on the rotating disc to 8 poles gives 1250N, so by taking this value lets calculate the excitation current.

4.3.2 Excitation Current

From fundamental principles of electromagnetism (William H. and Jr. John. A., 2006); the force generated by single core can be calculated as;

$$F = \frac{A \times \mu_0 \times (Ni)^2}{2 \times l_g^2}$$

where;

- $F =$ force generated by single core,
- $A_p =$ area of pole face

Considering the pole face is circular in shape; the area of the pole face can be calculated using the following formula;

$$A_p = \pi * \frac{(d_p)^2}{4}$$

Substituting diameter of the pole face in the equation; area of pole face gives;

$$A_p = \pi * \frac{0.05m^2}{4} = 0.0019635m^2$$

- $\mu_0 =$ permiability of air $= 4\pi \times 10^{-7} \frac{N}{A^2}$,
- $N =$ number of turns,
- $i =$ current,
- $l_g =$ airgap

Substituting the braking force requirement for one pole is 1250N.exitation current can be calculated; so that, solving for excitation current for one pole gives;

$$i = \sqrt{\frac{F * (2 * G^2)}{A * \mu_0 * N^2}}$$

Therefore, substituting the values and assumptions gives;

$$i = \sqrt{\frac{1250N * (2 * (0.001m)^2)}{0.001935m^2 * 4 * \pi * 10^{-7} \frac{N}{A^2} * 50^2}} = 20.27A$$

Since the current reaches 20A, the required wire diameter becomes quite large. This not only takes up more space but also results in high resistance, which can hinder the coil from producing the desired magnetic flux and braking force. To mitigate this, let's increase the assumed number of turns from 50 to 100. This change will reduce the wire diameter and resistance, thereby enhancing the coil's ability to generate the necessary magnetic flux and braking force. By relating the number of turns and current, the new excitation current can be obtained;

$$N_1 i_1 = N_2 i_2$$

Then by substituting the previous assumed number of turns, the calculated current and new assumed number of turns; the new excitation current gives;

$$i_2 = \frac{N_1 i_1}{N_2} = \frac{50 * 40A}{100} = 10A$$

Therefore, total design number of turns for 8 poles is 800 and design maximum current is 12A.

4.3.3 Design of coil

From American wire gauge table (See Appendix 1), the diameter of the wire and the area of the wire for maximum 12A is obtained as follows;

$$AWG 11, d_{wire} = 2.30378mm = 0.00230378m, A_{wire} = 4.17 \times 10^{-6}m^2$$

Calculation of the length of wire;

Since the winding geometry is considered as cylindrical in shape with the height of 0.10m and the diameter of the coil = $d_{coil} = 0.02m$; the length of the wire can be calculated as;

$$L = \pi (d_{coil} + t_{wire}) \times N + 2\pi \times r_{coil} \times N \times h_{coil}$$

Where;

$L = \text{length of wire,}$

d_{coil} = coil diameter,

t_{wire} = thickness of the wire,

N = number of turns,

r_{coil} = coil radius,

h_{coil} = height of the coil

Therefore;

$$L = \pi (0.02m + 0.0023038m) * 100 + (2\pi * 0.01m * 100 * 0.10m) = 7.63m \text{ say } 8m$$

4.3.4 Resistance of the wire

Resistance is a fundamental characteristic of materials that describes their ability to impede the flow of electric current. It is represented by the symbol R and measured in ohms (Ω) (byjus.com, 2024). Therefore, from ohms law; resistance can be calculated as;

$$R = \rho_c \frac{L}{A_{wire}}$$

Where;

R = Resistance

ρ_c = resistivity of the wire (i.e. copper = $1.72 \times 10^{-8} \Omega - m$)

L = length of the wire

Therefore; putting the available data in to the equation becomes;

$$R = \frac{1.72 \times 10^{-8} \text{ ohm} - m * 8m}{4.17 \times 10^{-6} m^2}$$

$$\text{Then } R = 0.033 \Omega$$

4.3.5 Magnetic field Strength

The magnetic field strength measures the intensity of a magnetic field at a certain place in space. It is a measure of the magnetic force applied to a unit magnetic pole located at that point (Robert Sheldon, 2024). Therefore, Magnetic field strength for one pole can be calculated as;

$$H = \frac{i * N}{\text{Air gap}}$$

Substituting for value of current, air gap and number of turns, it gives;

$$H = \frac{12A * 100}{0.001m}$$

$$\text{then, } H = 1.2 \times 10^6 A/m$$

4.3.6 Magnetic flux density

Magnetic flux density, often known as B , is a basic concept in magnetic theory that describes the strength of a magnetic field in a certain region of space. It quantifies the amount of magnetic flux passing through a unit area perpendicular to the direction of the field of magnets, or it measures the quantity of magnetic field lines within a given location (electricalacademia.com, 2024). Therefore, magnetic flux density without considering reluctance can be calculated as follows;

$$B = \frac{\mu_0 * i * N}{\text{Air gap}} = \mu_0 * H$$

Based on magnetic circle theory, to calculate magnetic flux density, reluctance should be considered, which means the formula describes the magnetic flux density B in a coil when a conductive disc is rotating nearby. It considers two main factors which are the magnetomotive force generated by the solenoid and the influence of the rotating disc. The magnetomotive force is determined by the number of turns in the solenoid and the electric current passing through it. The rotating disc affects the magnetic field due to its conductivity and motion, which induces eddy currents that oppose the magnetic field. The formula accounts for the resistance to the magnetic field from both the air gap and the rotating disc, showing how these elements together determine the resulting magnetic flux density (Zhou et al., 2015), therefore it becomes;

$$B = \frac{Ni}{\left(\frac{l_g}{\mu_0}\right) + \sigma * a_d * r_p * t_{disc} * \omega}$$

Where;

$$N = \text{number of turns} = 800$$

$$t_{disc} = \text{thickness of rotating disc} = 0.012$$

$$l_g = \text{air gap} = 0.001$$

$\omega = \text{angular velocity} = 167.55 \text{ (rad/s)}$

$\sigma = \text{material conductivity} = 2.495 \times 10^7 \frac{A^2 \cdot s^3}{kg \cdot m^3}$; for Aluminium Alloy Disc 6061 and $5.96 \times$

$10^7 \frac{A^2 \cdot s^3}{kg \cdot m^3}$ for Copper Disc

$a_d = \text{distance from the center of the pole to the center of rotating disc}$

$r = \text{radius of pole face } 0.025m$

Then, substituting the values into the equation gives;

$$B = \frac{800 * 12A}{\left(\frac{0.001m}{4 * \pi * 10^{-7} Kg \cdot m / A^2 s^2} \right) + 2.495 \times 10^7 \frac{A^2 \cdot s^3}{kg \cdot m^3} * 0.135m * 0.012m * 0.025m * 167.55 \text{ rad/se}}$$

$$B = 0.056 \text{ or } \frac{Kg}{A^2} \cdot s^2 \text{ for aluminum alloy 6061}$$

$$\frac{800 * 12A}{\left(\frac{0.001m}{4 * \pi * 10^{-7} Kg \cdot m / A^2 s^2} \right) + 5.96 \times 10^7 \frac{A^2 \cdot s^3}{kg \cdot m^3} * 0.135m * 0.012m * 0.025m * 167.55 \text{ rad/se}}$$

$$B = 0.0236 \text{ say } 0.024 \text{ Tesla or } \frac{kg}{A^2 \cdot s^2} \text{ for copper}$$

4.3.7 Magnetic flux

Magnetic flux describes the amount of magnetic field going through a specific location. It is an indicator of the total number of magnetic field lines that penetrate a surface perpendicular to the direction of the magnetic field (Khanacademy.org, 2024). Therefore, Magnetic flux can be calculated using the following formula;

$$\Phi = B * A_{core}$$

$$\text{But; } A_{core} = A_p = \pi * r_{core}^2 = \pi * 0.025m^2 = 0.0019635m^2$$

Then; substituting the values in the equation gives;

$$\Phi = 0.1 \text{ Tesla} * 0.0019635m^2 = 0.00019635 \text{ Weber For aluminum Alloy 6061}$$

$$\Phi = 0.024 \text{ Tesla} * 0.0019635m^2 = 0.00047124 \text{ Weber for copper}$$

4.3.8 Current Density

Current density is a key term in electromagnetism that describes how electric current is distributed within a conductor. It is defined as the amount of electric current passing through a

unit cross-sectional area in the opposite direction of the current flow. In other words, it measures the amount of electric current present in a particular volume of material. It is influenced by several factors. These include the electrical conductivity of the material, the speed at which the disc rotates (angular velocity), and the strength of the magnetic field. Additionally, the distance between the center of the disc and the center of the magnetic pole affects the current density. When the disc spins in the magnetic field, the interaction between the moving charges in the disc and the magnetic field induces an electric current, with the intensity determined by these parameters.

Therefore, from magnetic circle theory Current density can be calculated using the following formula(Alexandre J., 2020);

$$\text{current density} = J_e = \sigma \times [a_d * \omega * B]$$

Where

J_e : Current density,

σ = electrical conductivity

$$\sigma = 2.495 \times 10^7 \text{ Ohm} - m^{-1} \text{ or } \left(\frac{A^2 \cdot s^3}{kg \cdot m^3} \right) \text{ for Aluminum Alloy 6061 disc and}$$

$$\sigma = 5.96 \times 10^7 \text{ Ohm} - m^{-1} \left(\frac{A^2 \cdot s^3}{kg \cdot m^3} \right) \text{ for Copper disc}$$

$$a_d = \text{distance between center of the disc and center of the pole} = 135\text{mm} = 0.135$$

$$\omega = \text{angular velocity,} = 1600\text{RPM} = 167.5\text{RPS}$$

B = magnetic flux density

Then substituting the values into equation gives the following results;

$$J_e = 2.495 \times 10^7 \frac{A^2 \cdot s^3}{kg \cdot m^3} * \left[0.135\text{m} * 167.5 \text{ RPS} * 0.056 \frac{kg}{A^2} \cdot s^2 \right]$$

$$J_e = 31,603,616.1 \frac{A}{m^2} \text{ for Aluminum Alloy 6061 disc}$$

$$J_e = 5.96 \times 10^7 \frac{A^2 \cdot s^3}{kg \cdot m^3} * \left[0.135\text{m} * 167.5 \text{ RPS} * 0.024 \frac{kg}{A^2} \cdot s^2 \right]$$

$$J_e = 32,354,575.2 \frac{A}{m^2} \text{ for Copper disc}$$

4.3.9 Power dissipation, braking torque and force

In electromagnet retarders, power dissipation refers to the amount of energy that is lost as heat in the system. This dissipation occurs due to the flow of current through the electromagnet's disc. The resistivity of the material, the density of the current, and the volume of the disc all contribute to this process. Essentially, as more current flows through the disc, more heat is generated, leading to higher power dissipation. Power dissipated can be calculated using again magnetic circle theory;

$$P_d = \rho * J_e^2 * V_{disc} = \rho * J_e^2 * A_{disc} * t_{disc}$$

Where;

$P_d = \text{power dissipated,}$

$\rho = \text{Electrical resistivity}$

$$\rho = 4.066 \times 10^{-8} \frac{\text{kg} \cdot \text{m}^3}{\text{A}^2 \cdot \text{s}^3}, \text{ for Aluminum alloy 6061 disc and}$$

$$\rho = 1.68 \times 10^{-8} \text{ for Copper disc}$$

$$A_{disc} = \text{area of rotating disc} = \pi * 0.170^2 = 0.09079\text{m}^2$$

$$t_{disc} = \text{thickness of rotating disc} = 0.012\text{m}$$

Therefore;

$$P_d = 4.066 \times 10^{-8} \frac{\text{kg} \cdot \text{m}^3}{\text{A}^2 \cdot \text{s}^3} * \left(31,603,616.1 \frac{\text{A}}{\text{m}^2} \right)^2 * 0.09079\text{m}^2 * 0.012\text{m}$$

Then, $P_d = 44,244.5917 \text{ watts for alminum alloy 6061 disc}$

$$P_d = 1.68 \times 10^{-8} \frac{\text{kg} \cdot \text{m}^3}{\text{A}^2 \cdot \text{s}^3} * \left(32,354,575.2 \frac{\text{A}}{\text{m}^2} \right)^2 * 0.09079\text{m}^2 * 0.012\text{m}$$

$$P_d = 19,160.196 \text{ watts for Copper disc}$$

In electromagnet retarders, power dissipation and torque are intimately related. When the retarder is engaged, it creates a magnetic field that induces eddy currents in nearby conductive materials, such as the rotor or driveshaft of the vehicle. These currents create resistance, generating braking torque that slows down the vehicle. The power dissipation is directly proportional to the torque produced; higher power dissipation results in greater braking torque. Therefore, the braking torque can be calculated using the following formula;

$$T_b = \frac{P_d}{\omega} = \frac{44,244.5917 \text{ Watts}}{167.55 \text{ rps}} = 264.067 \text{ N} - m \text{ for Alminum Alloy 6061 disc}$$

$$T_b = \frac{P_d}{\omega} = \frac{19,160.196 \text{ Watts}}{167.55 \text{ rps}} = 114.355 \text{ N} - m \text{ for Copper disc}$$

The braking force therefore can be calculated using torque formula;

$$F_b = \frac{T_b}{\text{disc radius}} = \frac{264.067 \text{ N} - m}{0.170 \text{ m}} = 1553.34 \text{ N for Aluminum Alloy 6061 Disc}$$

$$F_b = \frac{T_b}{\text{disc radius}} = \frac{114.355 \text{ N} - m}{0.170 \text{ m}} = 672.7 \text{ N for copper Disc}$$

To achieve optimal torque generation using an electromagnetic retarder, Design Expert software is employed to determine the best combinations of the number of turns, air gap, and current. These parameters are crucial for torque optimization, as they are calculated for each combination to find the most effective setup. The focus is on Aluminium Alloy 6061 and Copper. The ranges for the current (i), air gap (l_g), and the number of turns (N) are set as follows: 10mA to 19A, 0.0009m to 0.0015m, and 100 to 800 turns, respectively. Design Expert software conducts 19 iterations to identify the optimal torque value using the torque formula. The results of these calculations for each combination are presented in Table 4.1.

$$T_b = \rho * \omega * A_{disc} * t_{disc} * a_d^2 * \sigma^2 * \left(\frac{Ni}{\left(\frac{l_g}{\mu_0}\right) + \sigma * a_d * r_p * t_{disc} * \omega} \right)^2$$

Form table 4.1 it is found that 656.54Nm is the maximum Torque generation, which is found by taking N=900, current=16.704A and airgap=0.0012m.

Table 4. 1 Torque Optimization Iteration for Aluminium Alloy 6061

Runs	Current (A)	Air Gap (m)	Number of turns	Retarding Torque (Nm)
1	15	0.0009	800	419.46
2	15	0.0015	1000	576.67
3	8.29552	0.0012	900	161.91
4	16.7045	0.0012	900	656.54
5	12.5	0.0012	900	367.63
6	12.5	0.0012	900	367.63
7	10	0.0015	1000	289.66
8	12.5	0.0012	900	367.63
9	12.5	0.0012	900	367.63
10	12.5	0.0012	731.821	243.07
11	10	0.0015	800	185.386
12	12.5	0.0012	1068.18	517.89
13	10	0.0009	800	186.42
14	12.5	0.00170454	900	365.91
15	12.5	0.000695462	900	369.37
16	15	0.0015	800	417.12
17	15	0.0009	1000	655.41
18	10	0.0009	1000	291.29
19	12.5	0.0012	900	367.638

By using the same iteration for copper disc, the following results are obtained

Table 4. 2 Torque Optimization Iteration for copper Disc

Runs	Current-i (A)	Air gap-l_g (m)	Number of turns-N (-)	Torque- Tb(N-m)
1	15	0.0009	800	186.25
2	15	0.0015	1000	290.336
3	8.29552	0.0012	900	72.01
4	16.7045	0.0012	900	291.982
5	12.5	0.0012	900	163.5
6	12.5	0.0012	900	163.5
7	10	0.0015	1000	129.03
8	12.5	0.0012	900	163.506
9	12.5	0.0012	900	163.506
10	12.5	0.0012	731.821	108.11
11	10	0.0015	800	82.58
12	12.5	0.0012	1068.18	230.32
13	10	0.0009	800	82.77
14	12.5	0.00170454	900	163.18
15	12.5	0.000695462	900	163.83
16	15	0.0015	800	185.81
17	15	0.0009	1000	291.02
18	10	0.0009	1000	129.34
19	12.5	0.0012	900	163.506

As tabulated in table 4-2, the maximum retarding torque generation is obtained in the combination of (900,0.0012m,16.7045A) which is 291.98Nm.

As Tabulated again in Table 4.1 and 4.2, the maximum torque generation is registered at the same number of turns, current and air gap of 900,0.0012m,16.7045A respectively. But, according to retarding purpose aluminium alloy 6061 is better than that of copper material.

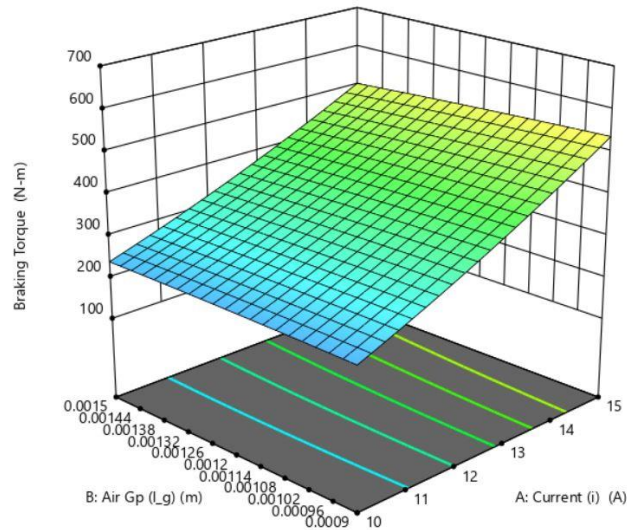


Figure 4. 2 Response 3D surface for Aluminium alloy 6061

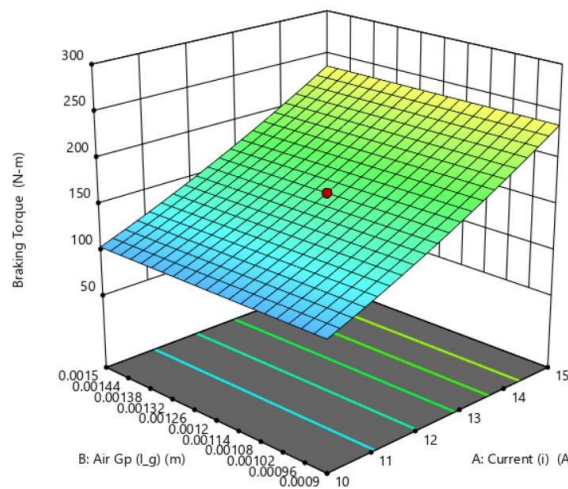


Figure 4. 3 surface response for Copper material

Figure 4.2 and 4.3 shows the relationship between braking torque, current, and air gap is depicted. As observed, the braking torque shows a direct proportionality to the current: as the current increases, the braking torque also increases. This trend is expected as the electromagnetic force, which contributes to the braking torque, is directly influenced by the magnitude of the current passing through the coil. The air gap, which is the distance between the rotor and the stator, also plays a significant role in the braking torque. Initially, as the air

gap increases, the braking torque shows a positive correlation and increases. This is because a larger air gap allows for a greater magnetic field interaction between the rotor and stator, enhancing the braking effect. However, this positive correlation only holds up to a certain point. Beyond this point, further increasing the air gap results in a decrease in the braking torque. The diminishing torque can be attributed to the fact that an excessively large air gap reduces the efficiency of the magnetic field interaction. The magnetic flux density diminishes with a larger gap, leading to a weaker electromagnetic force and, consequently, reduced braking torque.

Therefore, lets redesign by using these combination results. That is for the following values;

$$\text{Number of turns} = N = 900$$

$$\text{Air gap} = i = 0.0012m$$

$$\text{Current} = i = 16.7A$$

but, take the maximum current of 19A for selection of wire thickness.

Using maximum current 19A, AWG 9 having wire diameter or thickness of 0.00290576m, area of the wire is 0.00000663m² is selected (See Appendix 1).

Based on optimized number of turns value, that is 900 turns divide by 8 poles gives 113turns. So that, the wire length becomes;

$$L = \pi (0.02m + 0.00290576m) * 113 + (2\pi * 0.01m * 113 * 0.10m) = 11.1 \text{ say } 12m$$

Resistance of the conductive copper wire can be calculated as;

$$R = \frac{1.72 \times 10^{-8} \text{ ohm} - m * 12m}{4.17 \times 10^{-6} m^2} = 0.04949 \Omega$$

Therefore, re-calculated Magnetic flux density becomes;

$$B = \frac{Ni}{\left(\frac{l_g}{\mu_0}\right) + \sigma * a_d * r_p * t_{disc} * \omega}$$

Substituting the values in the equation it gives;

$$B = \frac{900 * 19A}{170260.43 \frac{kg}{A^3 \cdot s^2}} = 0.100 \text{ Tesla}$$

Current density which is used for determining power dissipation becomes;

$$J_e = 2.495 \times 10^7 \frac{A^2 \cdot s^3}{kg \cdot m^3} * \left[0.135m * 167.5 \text{ RPS} * 0.100 \frac{kg}{A^2 \cdot s^2} \right] = 56,435,028.75 \frac{A}{m^2}$$

Therefore, power dissipation is obtained as follows;

$$P_d = 4.066 \times 10^{-8} \frac{\text{kg} \cdot \text{m}^3}{\text{A}^2 \cdot \text{s}^3} * \left(56,435,028.75 \frac{\text{A}}{\text{m}^2}\right)^2 * 0.09079\text{m}^2 * 0.012\text{m}$$

$$P_d = 141,086.0705 \text{ Watts}$$

Retarding Torque generated by the retarder becomes;

$$T_b = \frac{P_d}{\omega} = \frac{141,086.0705 \text{ Watts}}{167.55 \text{ rps}} = 850 \text{ Nm}$$

Finally, the retarding force generated by retarder becomes;

$$F_b = \frac{T_b}{\text{disc radius}} = \frac{850\text{Nm}}{0.170\text{m}} = 5000\text{N}$$

4.3.10 Shaft with spur tooth design

To connect and transmit power from output of gear box flange in to the input of a propeller shaft flanges, there should be a shaft and flange in between, the spur teeth which is externally toothed on the shaft is necessary to be connected with internally toothed flanges at both ends, therefore shaft which have spur teeth at both ends are designed as follows;

- ✓ The material selected: Alloy steel
- ✓ Yield Tensile Strength (YTS)= 620MPs
- ✓ Assumed Shaft length (L) = 21cm = 210mm
- ✓ Assumed Torque:2000Nm
- ✓ RPM = 1600

From strength of materials;

Torsional shear stress can be calculated using the following formula.

$$\tau = \frac{T * r_{shaft}}{J}$$

Where;

τ = torsional shear stress

T = torque

$r_{shaft} = \text{shaft radius}$

$J = \text{polar moment of inertia,}$

To calculate the torsional shear stress, torque and radius are known, but polar moment of inertia is unknown,

therefore, polar moment of inertia for solid shaft can be calculated using the formula;

$$J = \frac{\pi d_{shaft}^4}{32}$$

Therefore, it becomes; $J = \frac{\pi * 0.035m^4}{32} = 1.473 \times 10^{-7}m^4$

Polar moment of inertia for hollow shaft can be calculated also using;

$$J = \frac{\pi}{32} * (d_{os}^4 - d_{is}^4)$$

Therefore; assume the inner diameter of the shaft is 0.01m

Then;

$$J = \frac{\pi}{32} * (0.035 m^4 - 0.01m^4) = 1.463 \times 10^{-7}m^4$$

Then, shear stress for solid shaft can be calculated as;

$$\tau_{solid} = \frac{2000Nm * 0.0175m}{1.473 \times 10^{-7}m^4} = 237.61Mp$$

Shear stress for hollow shaft can be calculated also;

$$\tau_{Hollow} = \frac{2000Nm * 0.0175m}{1.463 \times 10^{-7}m^4} = 239.2Mpa$$

Since the value of shear stress is less than the yield tensile stress, it shows that safe, let's check again by calculating the factor of safety.

Factor of safety for solid shaft can be calculated using the formula;

$$\text{Factor of safety} = \frac{\text{yield tensile strss}}{\text{calculated solid shaft shear stress}} = \frac{620Mpa}{237.61Mpa} = 2.609$$

Factor of safety for hollow shaft can be calculated also;

$$\text{Factor of safety} = \frac{\text{yield tensile stress}}{\text{calculated solid shaft shear stress}} = \frac{620\text{Mpa}}{239.2\text{Mpa}} = 2.591$$

The solid shaft has a higher factor of safety compared to the hollow shaft with a minimum value; however, both are safe for use. Despite this, the solid shaft is preferred for design purposes. For Spur tooth design (See Appendix 3)

4.3.11 Flange Design

- Assumed angular speed 1800RPM
- Diameter of the flange is 165mm the same as the diameter of the propeller shaft
- Torque = 2000NM
- Assume M10 bolt and number of bolts are 4.

Bolt spacing: in order to get bolt spacing the circumference of the flange should be divided by the number of bolts.

$$\text{Circumference} = \pi * 165\text{mm} = 518.36 \text{ mm}$$

Therefore, bolt spacing becomes; $\frac{518.4}{4} = 129.6\text{mm}$

Pitch diameter for the internal spur tooth on the flange is equal to module multiplied by number of teeth i.e.

$$D = 3\text{mm} * 10 = 30\text{mm}$$

Flange bending stress can be calculated using

$$\sigma_b = \frac{32 * N}{\pi D^3} = \frac{32 * 1800\text{RPM}}{\pi * (0.165\text{m})^3} = 4.081\text{MPa}$$

Since the bending stress of the flange is less than the yield tensile strength value, it can be concluded that the design is safe.

Bolt shear stress can be calculated also using the following formula i.e.

$$\tau = \frac{T}{A}$$

But Area can be calculated using, $A = \frac{\pi}{4} * d_{bolt}^2 = \frac{\pi}{4} * 0.01^2 = 7.854 \times 10^{-5}\text{m}^2$

Then bolt shear stress becomes;

$$\tau = \frac{2000Nm}{7.854 \times 10^{-5}m^2} = 25.46 MPa$$

Since bolt shear stress is less than yield tensile stress, it is safe.

Strength analysis for internal gear teeth can be calculated using flange bending stress and Lewis form factor. Assume Lewis form factor = 2.5

$$\text{contact stress} = \text{lewis form factor} * 4.081MPa = 2.5 * 4.01MPa = 10.025MPa.$$

Therefore, the contact stress is also less than yield tensile stress, it is safe.

Using again Lewis form factor, tooth bending stress can be calculated using the following formula.

$$\sigma_{tb} = \frac{2 * T}{\pi * d_{shaft} * m * (1 + \text{Number of teeth})}$$

Therefore, $\sigma_{tb} = \frac{2 * 2000Nm}{\pi * 0.035m * 0.003m * (1 + 10)} = 1.1 MPa$ which is also less than yield tensile strength, it is safe.

4.3.12 Bearing Selection

A mechanical component that reduces wear and friction between moving elements in machines is a bearing. It allows for efficient and smooth movement by supporting and guiding sliding or rotating components. Depending on the load capacity, speed, and motion type, different types of bearings, such as ball, roller, and plain bearings, are made for specialized applications (Testbook.com, 2024).

A. Ball Bearing: one of mechanical component that reduces friction between moving elements is a ball bearing. It produces a smooth rolling contact by using balls in place of a sliding contact. They are mostly utilized for light loading (Tameson.com, 2024).

B. Roller Bearing: A roller bearing is a type of rolling-element bearing, similar to a ball bearing, but instead of balls, it uses cylindrical rollers to minimize friction between moving parts. These can handle heavier loads than ball bearings but have more friction (Emersonbearing.com, 2024).

C. Thrust bearings: Unlike standard bearings that manage both radial and axial loads, thrust bearings are specifically designed to handle axial loads. They accomplish this by utilizing angled contact surfaces or flat thrust washers positioned between the rotating and

stationary parts. These surfaces evenly distribute the axial load, allowing for smooth rotation with minimal friction (globalspec.com, 2024).

D. Plain bearings: Plain bearings, also known as slide bearings or friction bearings, are the most basic and ancient type of bearing. Instead of using balls or rollers like rolling-element bearings, they function by facilitating a sliding contact between the shaft and the bearing surface. They are ideal for applications with low loads (bearingtips.com, 2024).

From bearing types, roller bearing is suitable for this design selection because of it can carry higher loads. To determine bearing load the following formula is used (Khurmi & Gupta, 2005).

$$F_{lb} = \frac{T}{r_s} * C_B$$

Where; $T = \text{torque} = 2000Nm$, $r_s = \text{radius of shaft} = 0.0175m$, $C_B = \text{bearing friction coefficient} = 0.01 - 0.02$ take 0.02

$$F_{lb} = \frac{2000Nm}{0.0175m} * 0.02 = 22857N$$

Based on the diameter of shaft and the bearing load, i.e. is 35mm and 22857N respectively, NU1007 bearing is selected (NSK.com, 2024).

4.4 CAD Modelling of Electromagnetic Retarder

Based on analytical calculations and assumption the following part components are modelled using SOLIDWORKS CAD software.

4.4.1 Single Stator and poles

Stator is one electromagnetic retarder part which holds poles, bearing and it is not movable like rotating disc it is fixed on chassis. Figure 4.4, shows 3D model of single stator holding 8 poles.

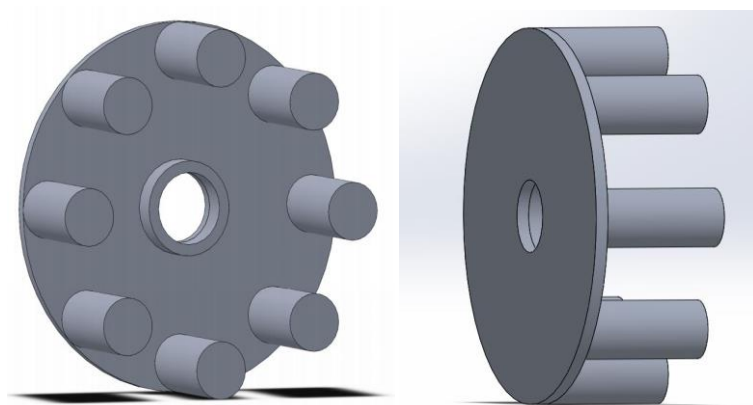


Figure 4. 4 Modelled stator and poles

4.4.2 Single Rotating Disc model

The other component of the electromagnetic brake retarder is rotating disc, which is used for generation of eddy current, the generated eddy current creates its own magnetic field so that it opposes the normal magnetic field, so that braking torque or force is generated. Figure 4.5, shows 3D model of rotating disc that is used for generation of braking torque.

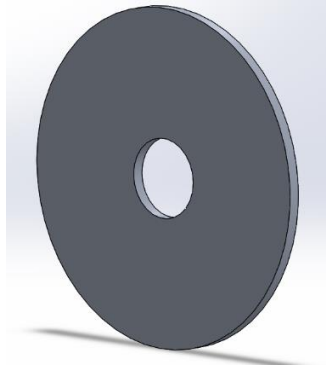


Figure 4. 5 Rotating disc

4.4.3 Shaft model

Figure 4.6 shows, a 3D modelling of a shaft which have spur tooth at both ends.

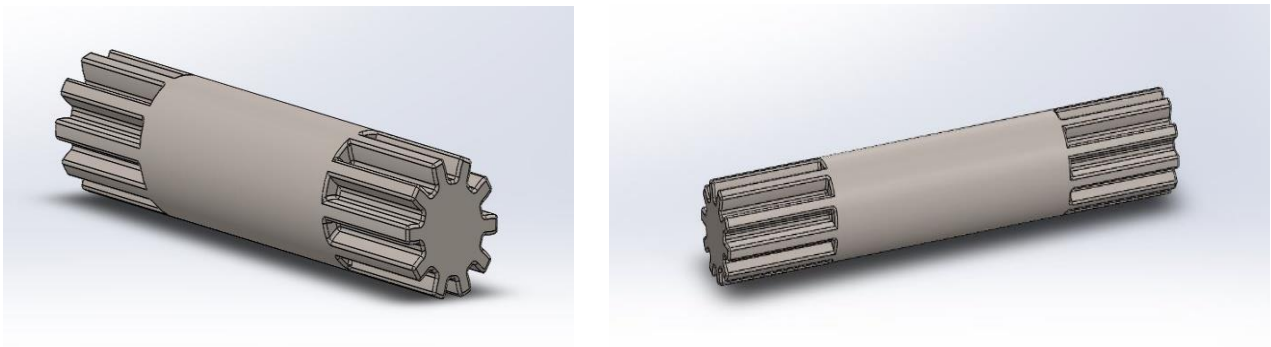


Figure 4. 6 Shaft with spur tooth at both ends

4.4.4 Flange with Internal Gear

Flange is necessary for strength and connecting one shaft to other shaft, or from one output system to other input system. In this case, it is connected with gear box output flange, then this flange is connected via internal spur tooth with shaft having external tooth, which is illustrated

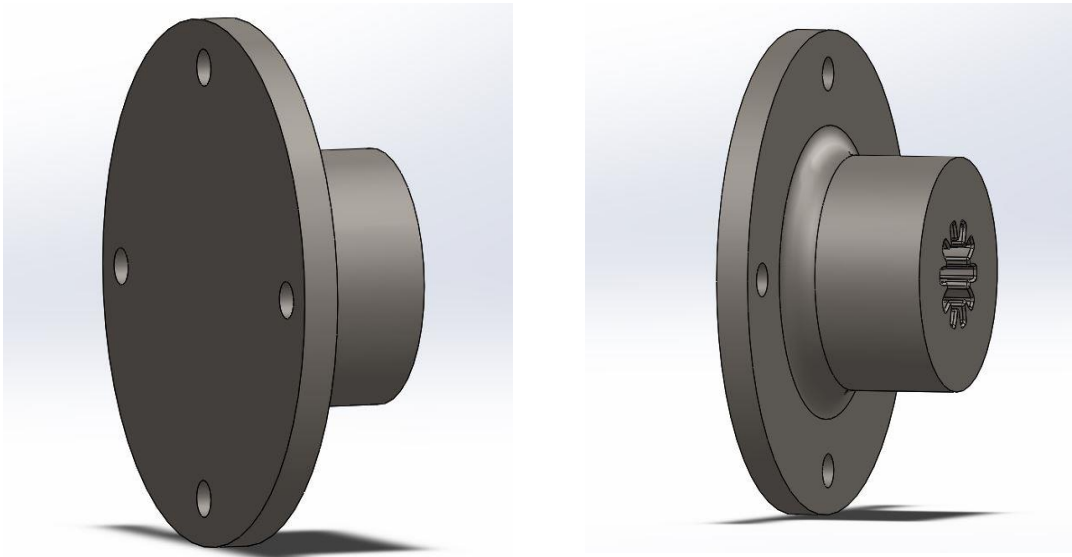


Figure 4. 7 Flange 3D model

in figure 15 to one end (from stator side), and the put of retarder flange at rotating disc side, is connected with propeller shaft. Figure 4.7, shows the 3D model of flange.

4.4.4 Roller Bearing

Roller Bearing is selected based on the maximum torque, angular speed and space availability. Figure 4.8 shows, bearing which is useful to hold and support the shaft.



Figure 4. 8 Roller Bearing

4.4.5 Assembly 3D modelling

Figure 4.9 shows assembled single stator single rotating disc electromagnetic retarder system.

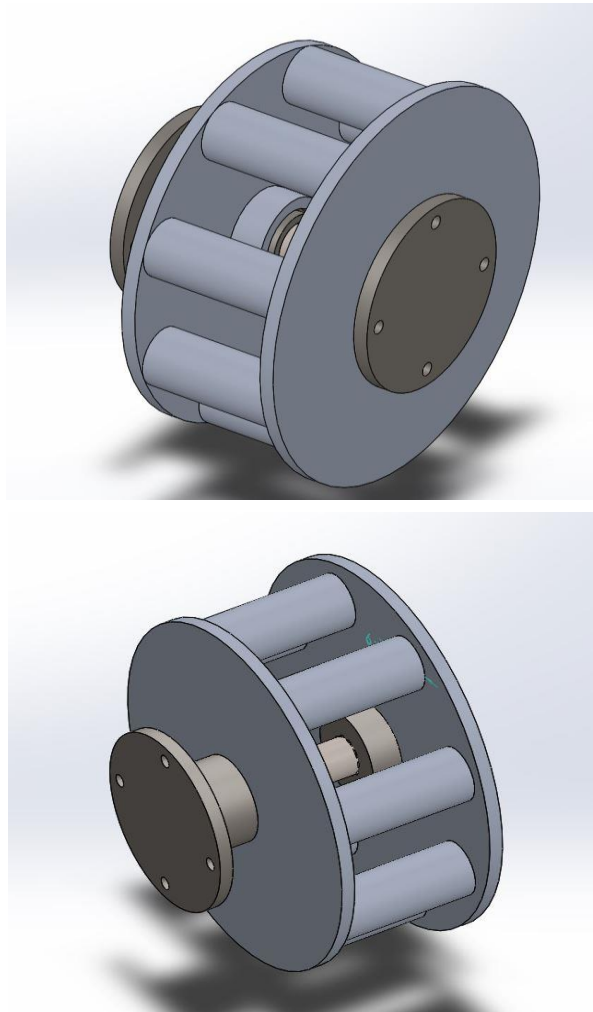


Figure 4. 9 Assembly of Single stator-rotor of electromagnetic retarder

CHAPTER FIVE

RESULT AND DISCUSSION

5.1 Analytical Design Outcome

The following table 5.1 shows the final result of design outcome.

Table 5. 1 design general results for electromagnetic brake retarder.

Description	Result
Calculated vehicle required torque	1700 N-M
Calculated vehicle required force	10 KN
Number of turns	900
Excitation current	19A
Wire gauge	AWG 9
Wire thickness	0.00290576m
Wire diameter	0.00000663m ²
Length of wire	12m
Resistance	0.04949 Ω
Magnetic flux density	0.100 <i>Tesla</i>
Current density	56,435,028.75 $\frac{A}{m^2}$
Power dissipation	141,086.0705 <i>Watts</i>
Generated retarding torque	850 <i>Nm</i>
Generated retarding force	5kN
Retarding efficiency	50%

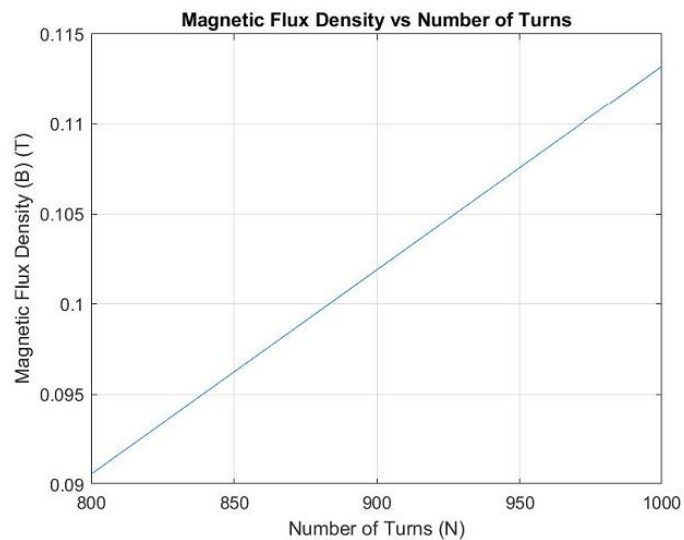


Figure 5. 1 Magnetic Flux Density vs Number of Turns

Figure 5.1 shows that as the number of turns in a coil increases, the magnetic flux density also increases.

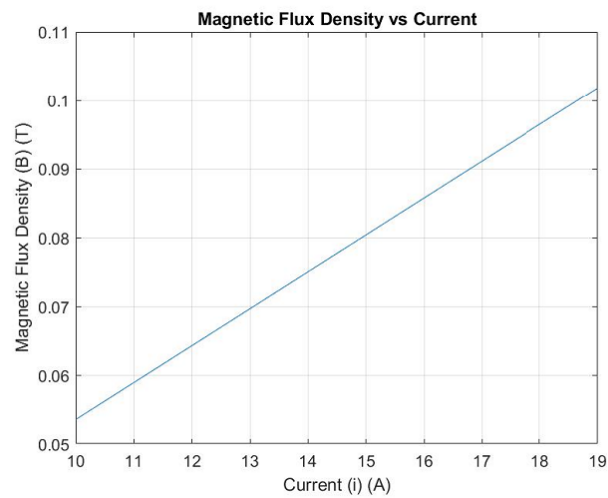


Figure 5. 2 Magnetic Flux Density vs Current Relation

Figure 5.2 shows, a graph having a linear relationship, which means the magnetic flux density increases proportionally with the current. This aligns with Ampere's Law, which states that the magnetic field created by an electric current is proportional to the size of that current.

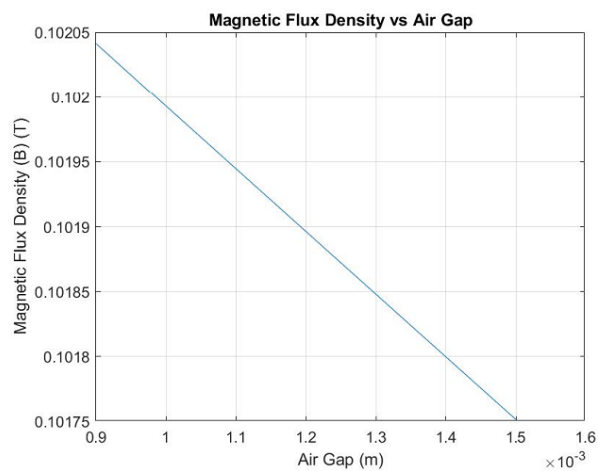


Figure 5. 3 Magnetic Flux Density vs Air gap Relation

Figure 5.3 shows the inverse relation between magnetic flux density and air gap. This means that as the air gap increases, the magnetic flux density decreases. An eddy current retarder uses a magnetic field to induce eddy currents in a conductive disk. The eddy currents create a magnetic field that opposes the original magnetic field, according to Lenz's law. This opposing magnetic field weakens the magnetic field in the air gap, the space between the rotor and the stator of the retarder.

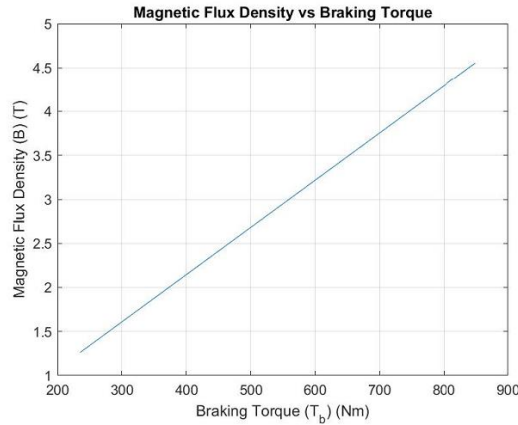


Figure 5. 4 Magnetic Flux Density vs Braking Torque Relation

Figure 5.4 shows a positive correlation between magnetic flux density (B) and braking torque (T). This means that as the magnetic flux density increases, the braking torque also increases. Because, an eddy current retarder uses a magnetic field to induce eddy currents in a conductive disk, the interaction between the magnetic field and the eddy currents creates a drag force, which is what creates the braking torque. A stronger magnetic field will induce stronger eddy currents, leading to a greater drag force and therefore higher braking torque.

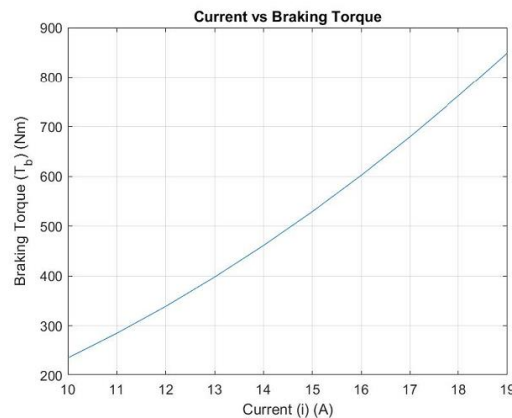


Figure 5. 5 Current vs Braking Torque relation

Figure 5.5 shows a positive correlation between current and braking torque. This means that as the current increases, the braking torque also increases. According to Ampere's Law, a higher current will result in a stronger magnetic field. In an eddy current brake, a stronger magnetic field will cause stronger eddy currents to be induced in the rotor disc. These eddy currents will then interact with the magnetic field to create a drag torque, which is what slows down the rotation of the shaft.

The excitation current required for retarding is determined to be 16.7A through the use of design expert combination methods for optimum torque generation. However, when selecting the appropriate wire gauge, a value of 19A was used, thus setting the maximum current for this design as 19A. This design choice results in a significant reduction in power consumption. When compared to data from reviewed articles, where excitation currents ranged from 30A to 50A (Xia et al., 2013)(K. Zhang et al., 2014)(Alexandre J., 2020).

Additionally, the magnetic flux density achieved in this design is 0.1 Tesla. According to previously reviewed articles, the maximum magnetic flux density achieved was 1.95 Tesla. While a higher magnetic flux density would lead to greater eddy current torque generation, it would also require a much higher excitation current. Therefore, although this design generates a lower magnetic flux density, it benefits from a significantly reduced current requirement, balancing efficiency and effectiveness.

In terms of performance metrics, the vehicle's required braking force and torque are calculated to be 10 kN and 1700 Nm, respectively. The retarding system designed in this study generates a retarding force of 5 kN and a torque of 850 Nm. This indicates that the retarding system is capable of achieving 50% of the necessary braking force and torque, effectively providing half of the total braking requirement.

5.2 Static Simulation Outcome

In the previous chapter the 3d modelling of electromagnetic retarder was presented for shaft, flange, stator and rotating disc components, these components are then simulated using ANSYS 2023 Student version simulation software.

5.2.1 Shaft

Since the shaft is rotating part of the system; taking the two ends as boundary condition, and maximum torque of 2000Nm is taken as input. So that considering maximum yield strength of steel alloy material the following results are obtained for total deformation, equivalent strain and stress. As shown in figure 5.6, the total deformation, maximum equivalent stress results; 0.027113mm and 105.35 Mpa respectively. The maximum equivalent strain as illustrated in figure 5.7, becomes 0.00062708mm.

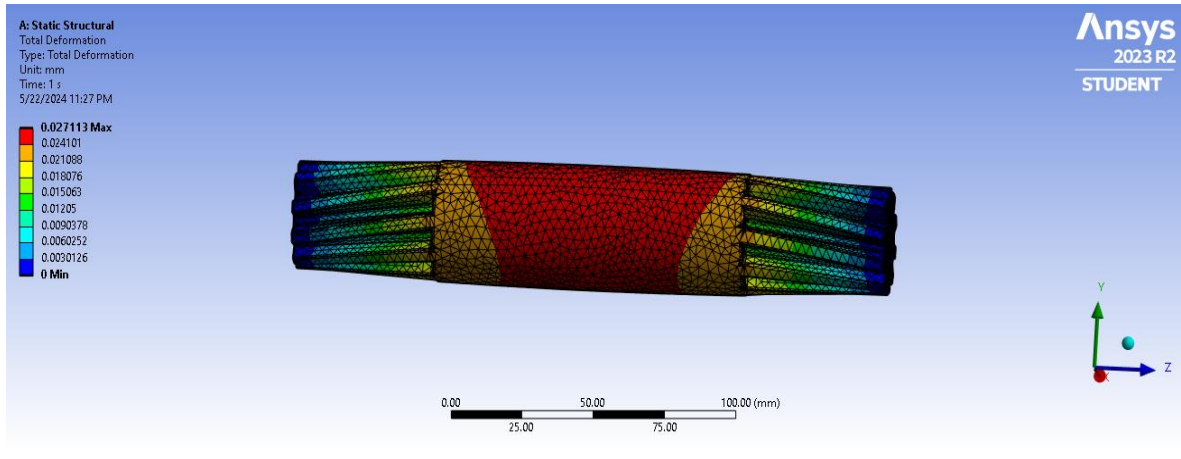


Figure 5. 6 Total Deformation and equivalent stress

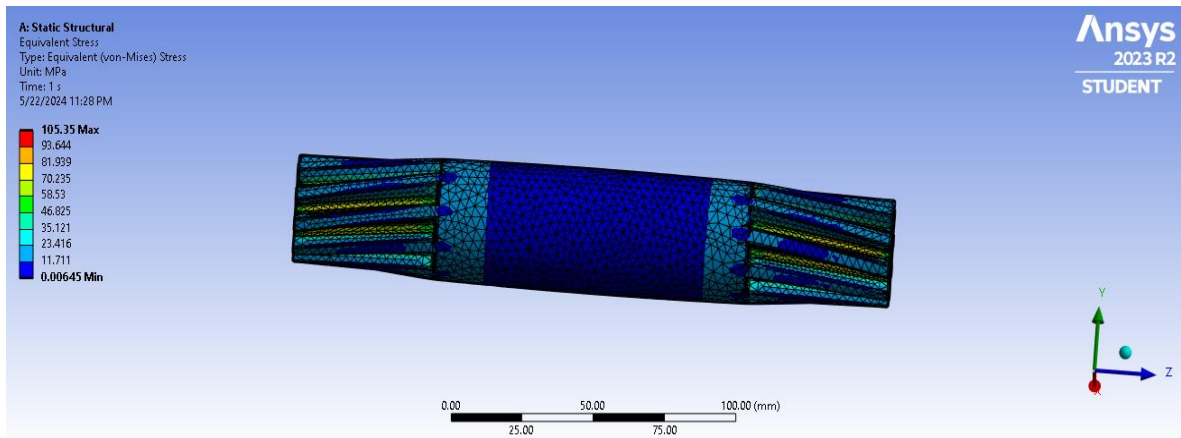
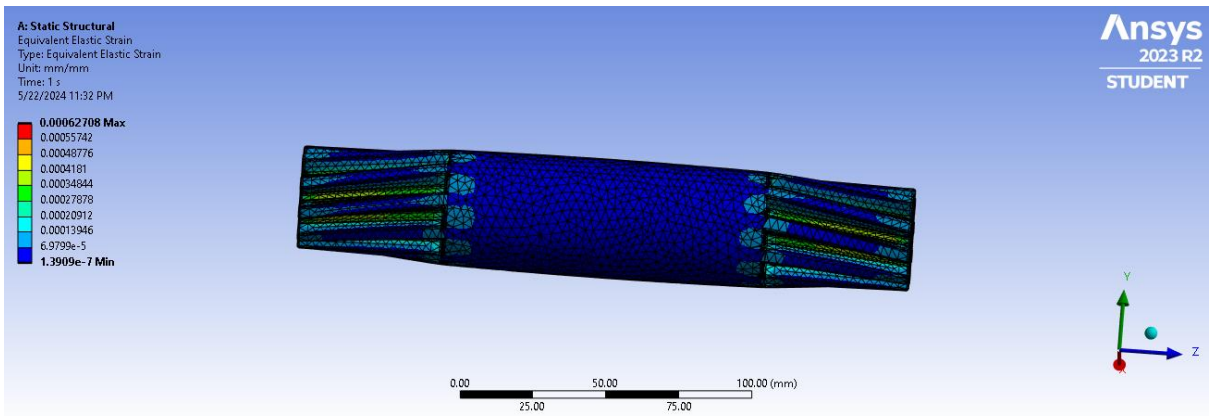


Figure 5. 7 Equivalent strain result



5.2.2 Flange

The flange also is a rotating part of the system; taking the internal gear and the face of the flange as boundary condition, and is taking maximum torque of 2000Nm as input, considering maximum yield strength of steel alloy material, the following results are obtained for total deformation as shown in figure 5.3.

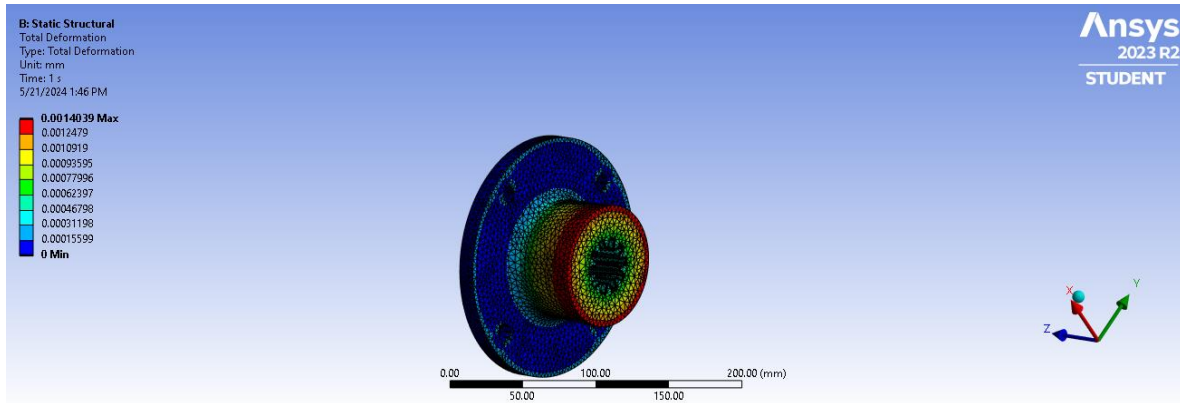


Figure 5. 8 Total deformation simulation

In figure 5.8, the colours gradient on the flange represents the amount of deformation with red areas showing the most significant deformation (0.0014039 mm) and blue areas showing no deformation. (0.000 min).

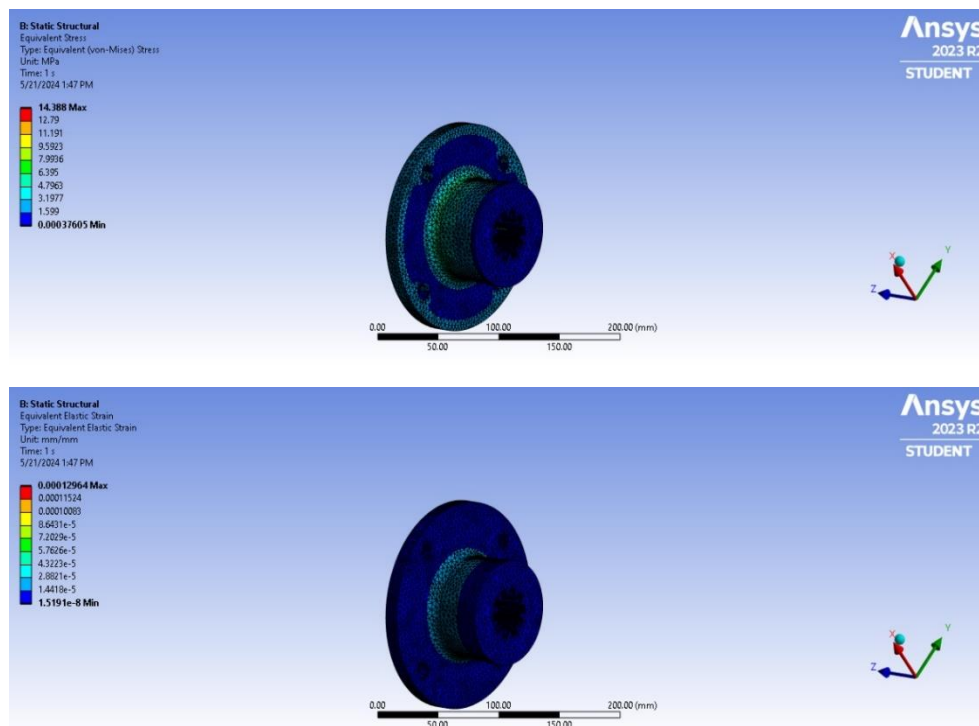


Figure 5. 9 Equivalent stress and strain result of Flange simulation

As shown in figure 5.9 The colour gradient on the flange represents the equivalent stress, with red areas showing the highest stress (14.388 MPa) and blue areas showing the lowest stress (0.00037605 MPa). in the case of equivalent elastic strain, with red areas indicating the most strain (0.00012964 mm/mm) and blue areas indicating the least strain (1.5191e-8 mm/mm).

5.2.3 Rotating disc

The disc that generate braking force is also subjected to rotational movement so, that the boundary condition for the disc is at the centre, or the disc is fixed at the centre and, by applying 4mm mesh and 2000Nm torque on the disc, then the following results are obtained. Figure 5.10 shows the result for total deformation the colour gradient tells us the amount of total

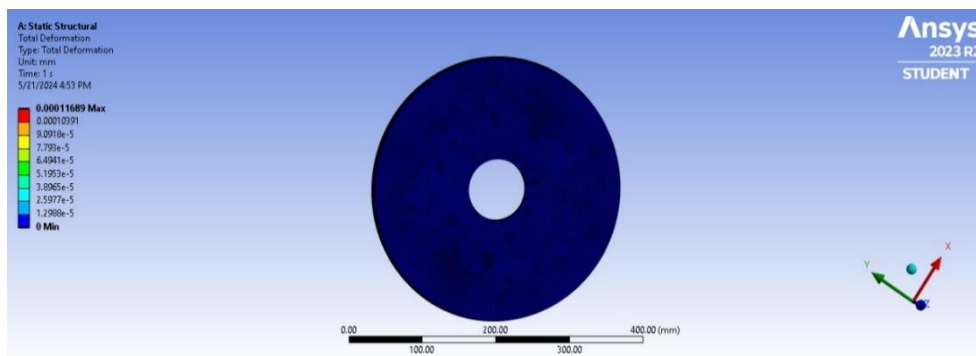


Figure 5. 10 Total deformation result for rotating disc simulation

deformation the object has undergone, with red areas showing the most significant deformation of 0.00011689 mm and blue areas showing the least deformation of 0mm.

In figure 5.11 shown, different colours shown in the rotating disc represents the amount of strain with red areas showing the most strain (6.3426e-6mm) and blue areas showing the least strain (1.4879e-6mm). Strain is the indication of how much the material has deformed from its original shape.

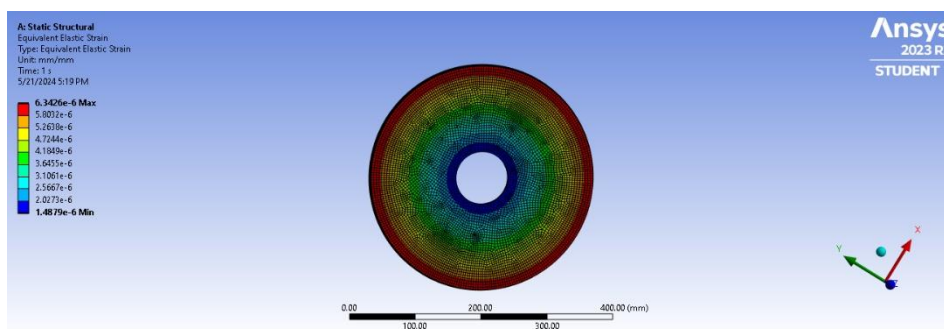


Figure 5. 11 Equivalent strain result of rotating disc simulation

Figure 5.12 shows the equivalent stress of rotating disc simulation; the red areas represent the highest stress (14.388 MPa) and are located on the edge of the flange.

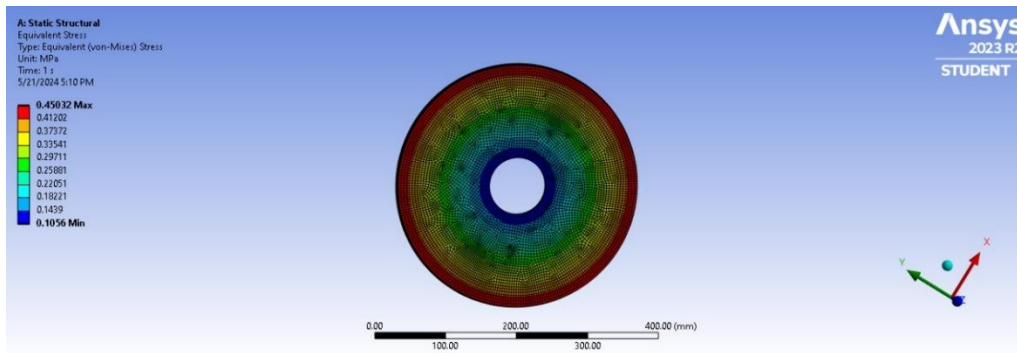


Figure 5. 12 Equivalent stress result for rotating disc simulation

5.2.4 Stator with Poles

Taking the stator material steel alloy, and subjecting the stator for 12.5 KN force, and by taking the stator disc faces as boundary condition, the following result is obtained.

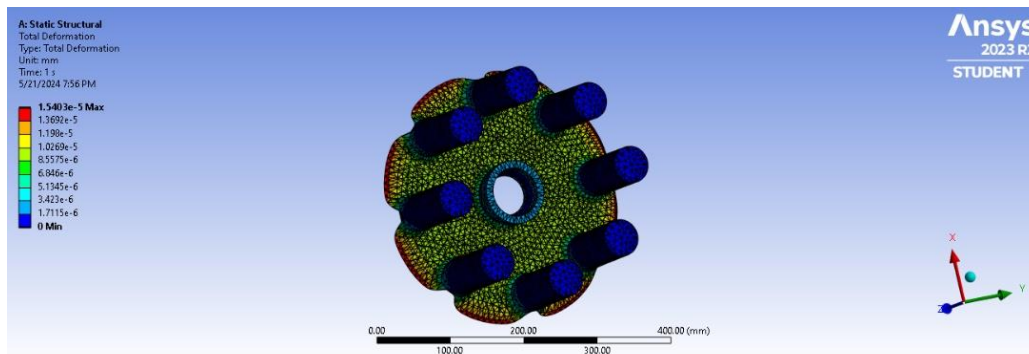


Figure 5. 13 Total deformation result

Figure 5.13 shows the result of stator with poles simulation; total deformation becomes 0.000015403mm.

Figure 5.14 and 5.15 shows, equivalent stress and strain simulation for stator with pole component, the maximum equivalent stress result becomes 0.28375 Mpa with maximum equivalent elastic strain of 0.0000014188mm.

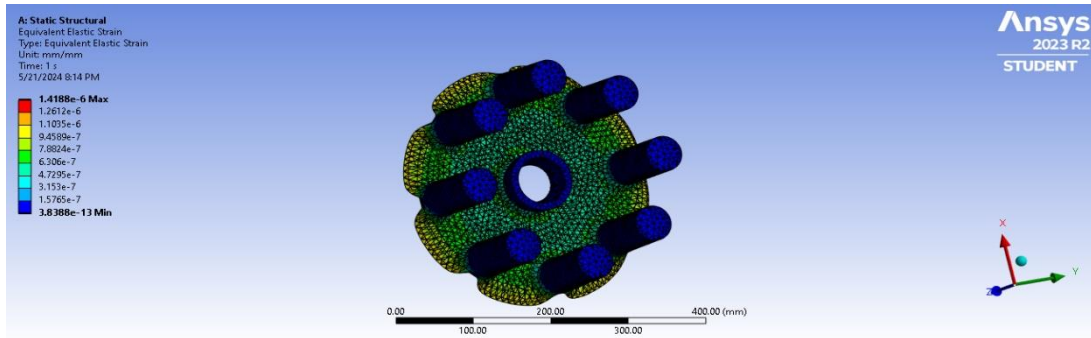


Figure 5. 14 Equivalent strain result for stator

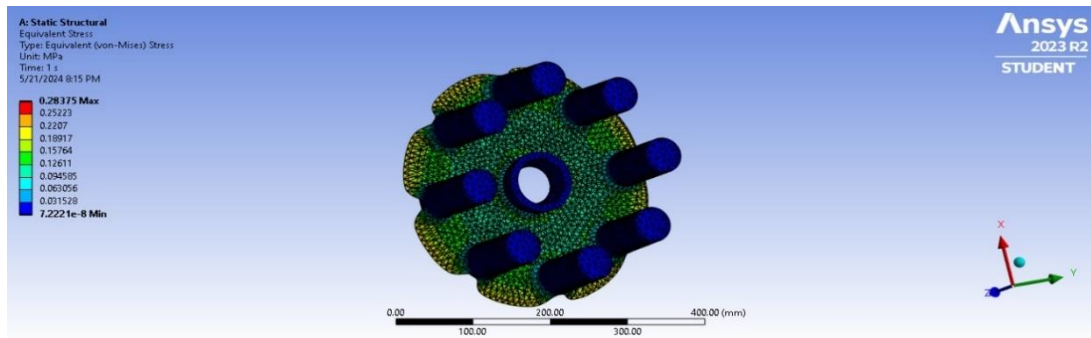


Figure 5. 15 Equivalent stress simulation result of stator with pole

Generally, the simulated equivalent stresses for the shaft, flange, and stator are 105.35 MPa, 14.388 MPa, and 0.28375 MPa, respectively. These values are well below the yield strength of 620 MPa for alloy steel, demonstrating that the material can safely withstand the applied torque. Similarly, the equivalent stress for the rotating disc is 14.388 MPa, which is much less than the yield strength of 276 MPa for aluminium alloy 6061. This confirms that the design of the rotating disc is secure and capable of handling the stresses it will encounter.

CHAPTER SIX

CONCLUSION AND RECOMMENDATION

6.1 Conclusion

In conclusion, now and then braking while driving downhill or uphill leads to brake fading, to minimize these frequent braking, additional braking mechanism makes it essential for heavy duty vehicles. Because of noiseless operation, simple structure and low-cost issues Electromagnetic brake retarder makes it important point to be added as additional auxiliary feature on the HOWO 336 dump truck, which is widely available vehicle in this country for construction and other purposes. Bearing this in mind, electromagnetic brake retarder is designed and analysed with different manual calculation and software simulation.

According to design results, the excitation current required for retarding is determined to be 16.7A using a design expert combination for optimal torque generation. However, for selecting the wire gauge, a maximum current of 19A was used.

The magnetic flux density obtained is 0.1 Tesla, whereas the maximum reported in previous studies was 1.95 Tesla. Although higher magnetic flux densities result in greater eddy current torque generation, they also require higher excitation currents.

The vehicle's required braking force and torque are calculated to be 10 kN and 1700 Nm, respectively, while the system developed in this study generates 5 kN of force and 850 Nm of torque. This indicates that the retarding system can achieve 50% of the required braking capacity, effectively contributing to vehicle braking with reduced power consumption and excitation current. Additionally, the simulation results for total deformation, equivalent strain, and stress on the electromagnetic retarder components (shaft, flange, rotating disc, and stator) show positive outcomes. The stress levels in each component remain well within their respective safe operational limits compared to their yield strengths.

6.2 Recommendation and future work

6.2.1 Recommendation

It is recommended that Sinotruck companies to consider incorporating the electromagnetic brake retarder into their HOWO 336 dump trucks. This addition could significantly reduce the need for frequent braking, thereby decreasing wear and tear on the service brakes. As a result, maintenance costs associated with brake system repairs and replacements would be minimized. Furthermore, by alleviating the load on the primary braking system, the electromagnetic

retarder would extend the service life of the brakes, enhancing overall vehicle efficiency and reliability. Implementing this technology would offer multiple benefits. Firstly, it would improve safety by providing consistent braking performance, especially on downhill and uphill routes where conventional brakes might experience fading. Secondly, the reduced strain on the service brakes would lead to lower maintenance costs over the vehicle's lifetime, as the brakes would require fewer repairs and replacements. Additionally, the overall downtime for brake maintenance would be reduced, increasing the operational availability of the trucks.

6.2.2 Future Work Recommendation

- ✓ It is recommended to conduct comprehensive testing of the electromagnetic brake retarder system to evaluate its efficiency for the specified vehicle, i.e. for HOWO 336 dump truck. This testing should be carried out in a controlled environment, such as a test bed or laboratory setting, to ensure accurate and reliable results.
- ✓ Assessing the retarder efficiency by combining different aluminium alloys for better retarding torque generation.

REFERENCES

- Alexandre J. (2020). Designing an Eddy Current Brake for Engine Testing. *KnE Engineering*. <https://doi.org/10.18502/keg.v5i6.7094>
- Aravind, A., Akilesh, V. R., Gunaseelan, S., & Ganesh, S. (2007). Eddy Current Embedded Conventional Braking System. In *International Journal of Innovative Research in Science, Engineering and Technology An ISO* (Vol. 3297, Issue 7). www.saeindiaskcet.org
- Ashby, M. F. (1999). *Materials selection in mechanical design*. Butterworth-Heinemann.
- Atamnia, K., Lebaroud, A., & Adikari, S. (2021). Forward-Looking Model Dedicated to the Study of Electric Vehicle Range Considering Drive Cycles. *The Scientific Bulletin of Electrical Engineering Faculty*, 21(1), 52–59. <https://doi.org/10.2478/sbeef-2021-0011>
- Azom.com. (2024a). *Alloy Steel (UNS G86300)*. <https://www.azom.com/article.aspx?ArticleID=6689>
- Azom.com. (2024b). *Properties: An Introduction to Copper*. <https://www.azom.com/properties.aspx?ArticleID=597>
- Baharom, M. Z., Nuawi, M. Z., Priyandoko, G., & Harris, S. M. (2012). Eddy current braking experiment using brake disc from aluminium series of A16061 and A17075. *IOP Conference Series: Materials Science and Engineering*, 36(1). <https://doi.org/10.1088/1757-899X/36/1/012005>
- bearingtips.com. (2024). *Plain bearings: What are they? - Bearing Tips*. <https://www.bearingtips.com/plain-bearings/>
- Bharti, S., & Anand, M. (2020). Introduction to Electromagnetic Braking System. *International Research Journal of Engineering and Technology*. <https://www.electric-brake.com/>
- byjus.com. (2024). *Ohm's Law - Statement, Formula, Solved Examples, Verification, FAQs*. <https://byjus.com/physics/ohms-law/>
- Chowdhury, H., Juwono, R., Zaid, M., Islam, R., Loganathan, B., & Alam, F. (2019). An experimental study on of the effect of various deflectors used for light trucks in Indian subcontinent. *Energy Procedia*, 160, 34–39. <https://doi.org/10.1016/j.egypro.2019.02.115>
- CNHDT Group. (2023). *HOWO DUMP TRUCK-Products-China National Heavy Duty Truck Group Co., Ltd.* <https://www.sinotruckgroup.com.cn/product-6.html>

- electricalacademia.com. (2024). *Magnetic Flux Density | Definition and Formula*.
<https://electricalacademia.com/electromagnetism/magnetic-flux-density-definition-unit-formula/>
- Emersonbearing.com. (2024). *What Are Roller Bearings? | Types and Applications*.
<https://www.emersonbearing.com/products/roller-bearings/>
- Ergün, R. E., Uçar, M., Metin Ertunç, H., Cengiz, A., & Ergün, R. E. (2014). A development of electromagnetic retarder controller to stabilise vehicle speed by using PWM technique. In *Int. J. Heavy Vehicle Systems* (Vol. 21, Issue 2).
- FuelFlowPro.com. (2023). *Understanding Diesel Exhaust Brakes: How They Work And Their Benefits | FuelFlowPro*. <https://fuelflowpro.com/diesel-exhaust-brake/>
- globalspec.com. (2024). *Thrust Bearings Selection Guide: Types, Features, Applications | GlobalSpec*.
https://www.globalspec.com/learnmore/mechanical_components/bearings_bushings/thrust_bearings
- Göhring, E., Von Glasner, E.-C., & Mercedes-Benz, R. P. (2018). *Engine Braking Systems and Retarders-An Overview from an European Standpoint*.
- Grandi, G., Kazimierczuk, M. K., Massarini, A., Reggiani, U., & Sancineto, G. (2004). Model of laminated iron-core inductors for high frequencies. *IEEE Transactions on Magnetics*, 40(4 I), 1839–1845. <https://doi.org/10.1109/TMAG.2004.830508>
- Hu, D., Yan, Y., & Xu, X. (2019). Energy saving optimal design and control of electromagnetic brake on passenger car. *Mechanical Sciences*, 10(1), 57–70. <https://doi.org/10.5194/ms-10-57-2019>
- Iyul Nasruddin. (2023). *Brake-retarder*. https://upgradedvehicle.com/brake-retarder/#google_vignette
- Jin, Y., Li, L., Kou, B., & Pan, D. (2019). Thermal Analysis of a Hybrid Excitation Linear Eddy Current Brake. *IEEE Transactions on Industrial Electronics*, 66(4), 2987–2997. <https://doi.org/10.1109/TIE.2018.2847703>
- Kalaaji, J., & Madi, M. (2019). Reduction of disc brake fading using both design and material optimization. *MATEC Web of Conferences*, 261, 02004. <https://doi.org/10.1051/mateconf/201926102004>
- Karade, M., Nagre, A., Choudhary, D., & Sahu, Y. (2022). Electromagnetic Braking System. In *International Journal of Research in Engineering and Science (IJRES) ISSN* (Vol. 10). www.ijres.org
- Khanacademy.org. (2024). *What is magnetic flux? (article) | Khan Academy*.
<https://www.khanacademy.org/science/physics/magnetic-forces-and-magnetic-fields/magnetic-flux-faradays-law/a/what-is-magnetic-flux>

- Khurmi, R. S., & Gupta, J. K. (2005). A Text book of Machine Design. In *Engg. Services*.
- Kumar Maurya, V., Jalan, R., Agarwal, H. P., Abdi, S. H., Pal, D., Tripathi, G., & Raj, S. J. (2011). EDDY CURRENT BRAKING EMBEDDED SYSTEM. In *International Journal of Applied Engineering and Technology* (Vol. 1, Issue 1). <http://www.cibtech.org/jet.htm>
- Lai, L. L. (2024). *ELECTRIC AND MAGNETIC CIRCUITS AND FIELDS*.
- Lubin, T., & Rezzoug, A. (2015). 3-D Analytical Model for Axial-Flux Eddy-Current Couplings and Brakes under Steady-State Conditions. *IEEE Transactions on Magnetics*, 51(10). <https://doi.org/10.1109/TMAG.2015.2455955>
- Mupona, M. I., & Singh Tomar, R. (2013). Evaluation of Materials Suitable for Use in Eddy Currents Non-Contact Brakes Disc in Automobile Application. In *International Journal of Science and Research* (Vol. 5). www.ijsr.net
- Nategh, S., Krings, A., Huang, Z., Wallmark, O., Leksell, M., & Lindenmo, M. (2012). Evaluation of stator and rotor lamination materials for thermal management of a PMSRM. *Proceedings - 2012 20th International Conference on Electrical Machines, ICEM 2012*, 1309–1314. <https://doi.org/10.1109/ICEIMach.2012.6350046>
- NSK.com. (2024). *Deep Groove Ball Brgs. Self-Aligning Ball Brgs. Ball Brg. Units Plummer Blocks Roll-Neck Brgs. (4-Rows) Railway Rolling Stock Brgs. Accessories for Rolling Brgs. NSK Products and Appendices C1*. <http://www.nsk.com>
- Putra, M. R. A., Nizam, M., Tjahjana, D. D. D. P., & Prabowo, A. R. (2021). Mini Review on Eddy Current Brakes Parameter. *IOP Conference Series: Materials Science and Engineering*, 1096(1), 012027. <https://doi.org/10.1088/1757-899x/1096/1/012027>
- Robert Sheldon. (2024). *What is magnetic field strength? – TechTarget Definition*. <https://www.techtarget.com/whatis/definition/magnetic-field-strength>
- Routh, P. K., Sagar, P., Kumar, R., & Paul, S. (2008). ELECTROMAGNETIC BRAKING SYSTEM. *International Research Journal of Engineering and Technology*, 5744. www.irjet.net
- Sailesh, B., & Krishna, R. H. (2021). *Electromagnetic braking system*.
- Sakamo, H., Araki, K., Ishida, A., Sumio Kobayashi, antd, & Kuwahara, T. (2018). *Design of Permanent Magnet Type Compact ECB Retarder Reprinted from: Heavy Duty Veh~icle Braking and Steering (SP-I 307) Intern~ational Truck & Blus Meeting & Exposition*.


- Sari, N., Khoiro, M., Rohedi, A. Y., Yudoyono, G., & Pramono, Y. H. (2020). Power efficiency analysis in various types of coil design. *IOP Conference Series: Materials Science and Engineering*, 858(1). <https://doi.org/10.1088/1757-899X/858/1/012055>
- Smyth, W. R., & Aiee, N. (1942). *On Eddy Currents in a Rotating Disk*.
- Tameson.com. (2024). *Ball Bearing Types and Components | Tameson.com*. <https://tameson.com/pages/ball-bearing>
- telma.com. (2024). *Operating principle - Retarders - Telma S.A.S*. <https://www.telma.com/produits/fonctionnement>
- Testbook.com. (2024). *Bearings: Learn its Types, Pros, Cons, Equations & Applications*. <https://testbook.com/mechanical-engineering/bearings>
- thecartech.com. (2024). *Road loads*. http://www.thecartech.com/subjects/auto_eng/road_loads.htm
- Valvolineglobal.com. (2024). *What Is the Braking System and What Kind of Oil Does It Require? - Valvoline™ Global KSA - EN*. <https://www.valvolineglobal.com/en-ksa/what-is-the-braking-system-and-what-kind-of-oil-does-it-require/>
- Waloyo, H. T., Ubaidillah, Tjahjana, D. D. D. P., Nizam, M., & Koga, T. (2019). Mini review on the design of axial type eddy current braking technology. *International Journal of Power Electronics and Drive Systems*, 10(4), 2198–2205. <https://doi.org/10.11591/ijpeds.v10.i4.pp2198-2205>
- Wang, J., & Zhu, J. (2018). A simple method for performance prediction of permanent magnet eddy current couplings using a new magnetic equivalent circuit model. *IEEE Transactions on Industrial Electronics*, 65(3), 2487–2495. <https://doi.org/10.1109/TIE.2017.2739704>
- Wang, W. H., & Li, J. (2013). Study on matching electromagnet retarder for city bus with force analysis based on brake directional stability. *Advanced Materials Research*, 644, 288–293. <https://doi.org/10.4028/www.scientific.net/AMR.644.288>
- William H. and Jr. John. A. (2006). *Engineering Electromagnetics*. <http://www.uop.edu.pk/ocontents/EMT.pdf>
- Wm. T. Mcllyman. (2011). *Transformer and Inductor Design Handbook Fourth Edition*. https://api.pageplace.de/preview/DT0400.9781439836880_A31978815/preview-9781439836880_A31978815.pdf
- Xia, W., Tan, G., Wang, S., & Wang, J. (2013). Experiment study and design of self-excited eddy current retarder. *SAE Technical Papers*, 12. <https://doi.org/10.4271/2013-01-2825>

- Xometry.com. (2024). *Alloy Steel vs. Carbon Steel* | Xometry.
<https://www.xometry.com/resources/materials/alloy-steel-vs-carbon-steel/>
- Xuejun, L., Zongyin, W., Nianjiong, Y., & Cunxiang, L. (2017). Design and performance experiment of the self-excitation electromagnetic retarder. In *Acta Technica* (Vol. 62, Issue 5B). <http://journal.it.cas.cz570>
- Yañez-Valdez, R., Alva-Gallegos, R., Caballero-Ruiz, A., & Ruiz-Huerta, L. (2012). Selection of soft magnetic core materials used on an LVDT prototype. *Journal of Applied Research and Technology*, *10*(2), 195–205.
<https://doi.org/10.22201/icat.16656423.2012.10.2.409>
- Yasa, Y., Sincar, E., Ertugrul, B. T., & Mese, E. (2016). A multidisciplinary design approach for electromagnetic brakes. *Electric Power Systems Research*, *141*, 165–178. <https://doi.org/10.1016/j.epsr.2016.07.020>
- Yazdanpanah, R., & Mirsalim, M. (2015). Hybrid electromagnetic brakes: Design and performance evaluation. *IEEE Transactions on Energy Conversion*, *30*(1), 60–69.
<https://doi.org/10.1109/TEC.2014.2333777>
- Ye, L., Cao, M., Liu, Y., & Li, D. (2019). Multi-Field Coupling Analysis and Demagnetization Experiment of Permanent Magnet Retarder for Heavy Vehicles (MAY 2018). *IEEE Access*, *7*, 50734–50745.
<https://doi.org/10.1109/ACCESS.2018.2884236>
- Ye, L., Liu, Y., & Li, D. (2019). Optimization design and test of dual air-gaps and liquid-cooled eddy current retarder. *International Journal of Applied Electromagnetics and Mechanics*, *61*(2), 157–170. <https://doi.org/10.3233/JAE-180109>
- Ye, L., Yang, G., & Li, D. (2014). Analytical model and finite element computation of braking torque in electromagnetic retarder. *Frontiers of Mechanical Engineering*, *9*(4), 368–379. <https://doi.org/10.1007/s11465-014-0314-x>
- Zach, R. (2023, June 28). *What Is a Brake Retarder?* | *Vehicle Answers*.
<https://vehicleanswers.com/what-is-brake-retarder/>
- Zhang, K., Li, D., Du, X., & Zheng, R. (2014). Numerical analysis and experimentation of a novel self-excited and liquid-cooled eddy current retarder. *IEEE Transactions on Energy Conversion*, *29*(1), 196–203. <https://doi.org/10.1109/TEC.2013.2295218>
- Zhang, K., Li, D., Zheng, R., & Yin, W. (2015). Design and performance of a self-excited and liquid-cooled electromagnetic retarder. *IEEE Transactions on Vehicular Technology*, *64*(1), 13–20. <https://doi.org/10.1109/TVT.2014.2318059>
- Zhang, R. J. (2021). Structure design and coordinated control of electromagnetic and frictional braking system based on a hub motor. *Science Progress*, *104*(1).
<https://doi.org/10.1177/0036850421998483>
- Zhou, Q., Guo, X., Tan, G., Shen, X., Ye, Y., & Wang, Z. (2015). Parameter Analysis on Torque Stabilization for the Eddy Current Brake: A Developed Model, Simulation, and Sensitive Analysis. *Mathematical Problems in Engineering*, *2015*. <https://doi.org/10.1155/2015/436721>

APPENDIX 1: AWG TABLE

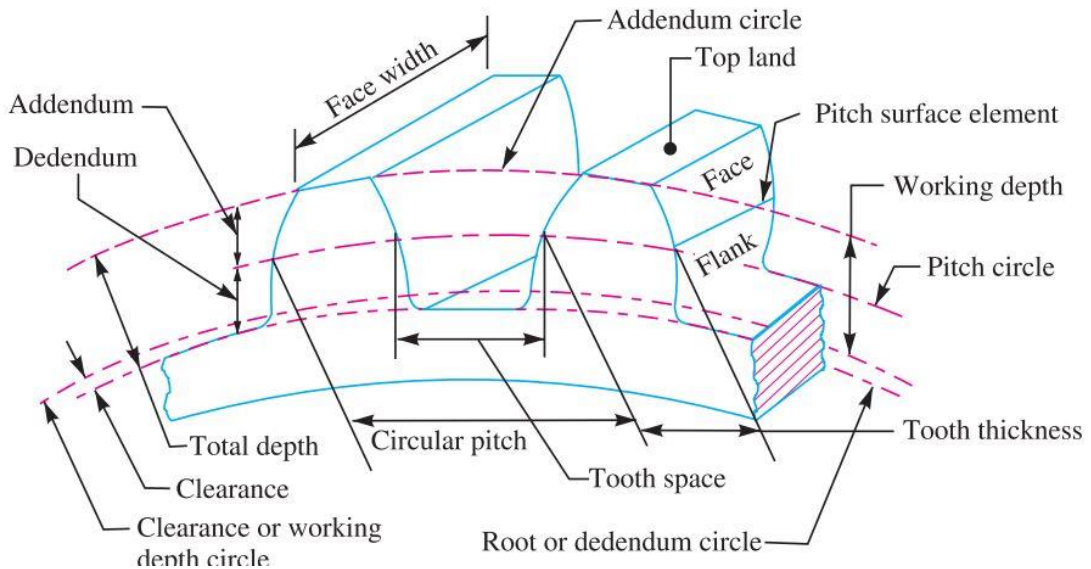
AWG	Diameter [inches]	Diameter [mm]	Area [mm ²]	Resistance [Ohms / 1000 ft]	Resistance [Ohms / km]	Max Current [Amperes]	Max Frequency for 100% skin depth
0000 (4/0)	0.46	11.684	107	0.049	0.16072	302	125 Hz
000 (3/0)	0.4096	10.40384	85	0.0618	0.202704	239	160 Hz
00 (2/0)	0.3648	9.26592	67.4	0.0779	0.255512	190	200 Hz
0 (1/0)	0.3249	8.25246	53.5	0.0983	0.322424	150	250 Hz
1	0.2893	7.34822	42.4	0.1239	0.406392	119	325 Hz
2	0.2576	6.54304	33.6	0.1563	0.512664	94	410 Hz
3	0.2294	5.82676	26.7	0.197	0.64616	75	500 Hz
4	0.2043	5.18922	21.2	0.2485	0.81508	60	650 Hz
5	0.1819	4.62026	16.8	0.3133	1.027624	47	810 Hz
6	0.162	4.1148	13.3	0.3951	1.295928	37	1100 Hz
7	0.1443	3.66522	10.5	0.4982	1.634096	30	1300 Hz
8	0.1285	3.2639	8.37	0.6282	2.060496	24	1650 Hz
9	0.1144	2.90576	6.63	0.7921	2.598088	19	2050 Hz
10	0.1019	2.58826	5.26	0.9989	3.276392	15	2600 Hz
11	0.0907	2.30378	4.17	1.26	4.1328	12	3200 Hz
12	0.0808	2.05232	3.31	1.588	5.20864	9.3	4150 Hz
13	0.072	1.8288	2.62	2.003	6.56984	7.4	5300 Hz
14	0.0641	1.62814	2.08	2.525	8.282	5.9	6700 Hz
15	0.0571	1.45034	1.65	3.184	10.44352	4.7	8250 Hz
16	0.0508	1.29032	1.31	4.016	13.17248	3.7	11 k Hz
17	0.0453	1.15062	1.04	5.064	16.60992	2.9	13 k Hz
18	0.0403	1.02362	0.823	6.385	20.9428	2.3	17 kHz
19	0.0359	0.91186	0.653	8.051	26.40728	1.8	21 kHz
20	0.032	0.8128	0.518	10.15	33.292	1.5	27 kHz
21	0.0285	0.7239	0.41	12.8	41.984	1.2	33 kHz
22	0.0254	0.64516	0.326	16.14	52.9392	0.92	42 kHz
23	0.0226	0.57404	0.258	20.36	66.7808	0.729	53 kHz
24	0.0201	0.51054	0.205	25.67	84.1976	0.577	68 kHz
25	0.0179	0.45466	0.162	32.37	106.1736	0.457	85 kHz
26	0.0159	0.40386	0.129	40.81	133.8568	0.361	107 kHz
27	0.0142	0.36068	0.102	51.47	168.8216	0.288	130 kHz

APPENDIX 2: SPECIFICATION OF HOWO 336 DUMP TRUCK

HOWO 6x4 336HP EURO II TIPPER (DUMP) TRUCK					
General Specification		General Performance Parameters			
Model	ZZ3257N3847A		Maximum Driving Speed	km/h	78
Series	HOWO		Average Fuel Consumption	liter/km	35liters/100km
Wheel Traction / Drive Style	6X4		Maximum Gradeability	%	≈30°
Full Load Mass Weight	kg	25000	Cargo Box Tilt Angle	%	45°-60°
Curb Mass/ Self Weight	kg	12270	Loading Capacity	kg	12600-25000
Steering Wheel Position	LHD/RHD	RHD (Right Hand Drive)	Cabin (HW76 Model)		
Engine					
Model	WD615.69		All-steel frame with 4-point support fully floating suspension and shock absorbers , Forward control 70° hydraulically tiltable cabin, 3-speed Twin arm wiper system, Laminated windscreen with casted-in radio aerial , AM/FM radio/cassette stereo player, Hydraulically damped adjustable driver's seat and rigid adjustable passenger seat with 3 point safety (seat) belt, Adjustable steering wheel, Heating and ventilating system, Exterior sun visor, Adjustable roof flap and Air horn		
Brand	SINOTRUK				
Displacement	9.726L				
Type	In-line, Six-cylinder, Four-stroke, Water-cooled, Direct Injection, Intercooled Turbocharged Diesel				
Engine Classification /	EURO II				
Bore/Stroke	mm	126/130			
Rated Horse Power	hp	336			
Net Power	KW/rpm	247KW/2200rpm			
Torque (Nm/rpm):	Nm/rpm	1350Nm @ 1100-1600rpm			
Clutch & Gear Box Systems					
Clutch	SINOTRUK's ϕ 430 diaphragm spring clutch				
Gear Box	SINOTRUK's HW19710 ,Manual Gearbox				
Gear Speed/Lever	10 forward/ 2 reverse				
Gear Ratio	14.28, 10.62, 7.87, 5.88, 4.38, 3.27, 2.43, 1.80, 1.34,				
Axle & Steering					
Steering Model	ZF8098				
Front Axle	SINOTRUK's HF9				
Rear Axle	SINOTRUK's HC16				
Ratio of Rear Axle	5.73				
Loading Capacity per Axle	front	9000kg			
	rear	(2x) 16000kg			
Brake System & Suspension					
Service Brake	dual circuit compressed air brake				
Auxiliary Brake	engine exhaust valve brake				
Parking Brake (Emergency Brake)	front	spring energy			
	rear	compressed air			
Suspension Type	front	10pcs leaf spring			
	rear	12pcs leaf spring			
Wheels & Tires					
Wheel Type	stud piloted 10 hole steel disc (20x8.50)				
Number of Tires	10+1 (spare tire)				
Tire Type/Size	12.00R20				
Track	front	2022mm			
	rear	1830mm			
Chassis & Dimensions					
Frame Details	High-strength 8+8/300mm and reinforced sub-frame				
	Overall Dimension	length	8600mm		
width		2500mm			
height		3400mm			
Wheelbase	mm	3825+1350			
Ground Clearance	mm	314			
	Vehicle Overhang	front	1500		
rear		1870			
Front/Approach angle	%	19°			
Rear/Departure angle	%	23°			
DUMP BOX SIZE					
LxWxH	5600*2300*1500 mm				
Volume	19.32m ³				
LIFT SYSTEM	Middle lift				
Floor Thickness	8mm				
Side Thickness	6mm				
Electrical System					
Battery	V/ah	24V/165ah			
	quantity	2			
Alternator	volts	28V			
Operating Voltage	volts	24V			
Fuel Tank					
Capacity	liters	300			
Shape / Structure	Rectangular / Aluminum				
SINOTRUK (CNHTC) have the right to change/upgrade the specification without prior notice, unless upon Final confirmation of Sale. Parameters are not listed, subject to the factory's standard					
PHOTO for reference only					
					

APPENDIX 3: SPUR TOOTH DESIGN FOR SHAFT

- ✓ Assumed Number of teeth = 10
- ✓ Assumed pitch diameter of the tooth = 30mm
- ✓ Assumed pressure angle = 20 degree (standard)
- ✓ Assumed Gear ratio is 1:1


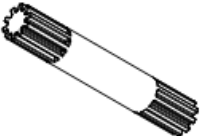



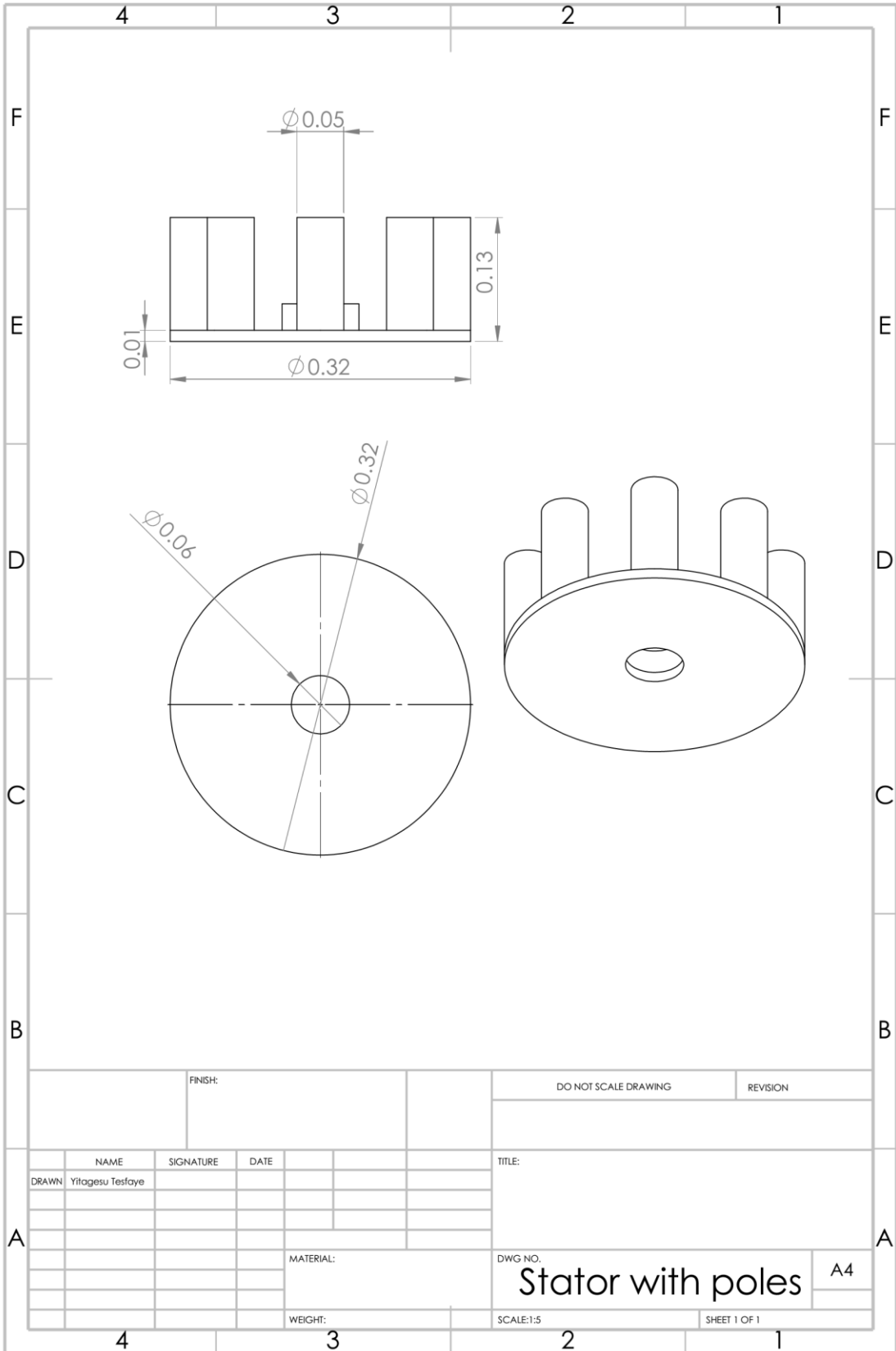
Spur tooth geometry (Khurmi & Gupta, 2005)

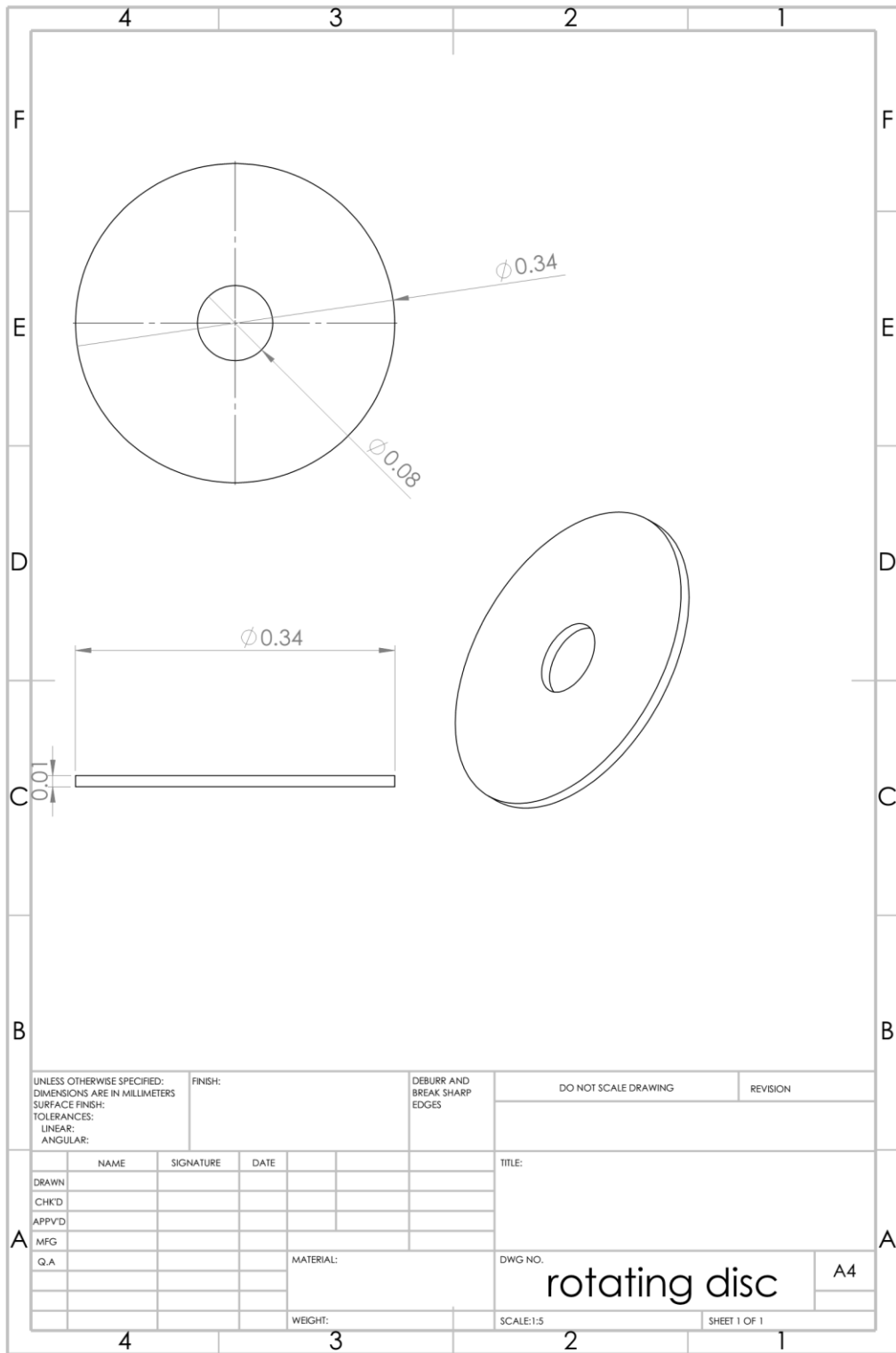
The figure above shows the geometry of spur tooth which have different profiles, Therefore, from tooth profile geometry of the spur gear; the following results are obtained;

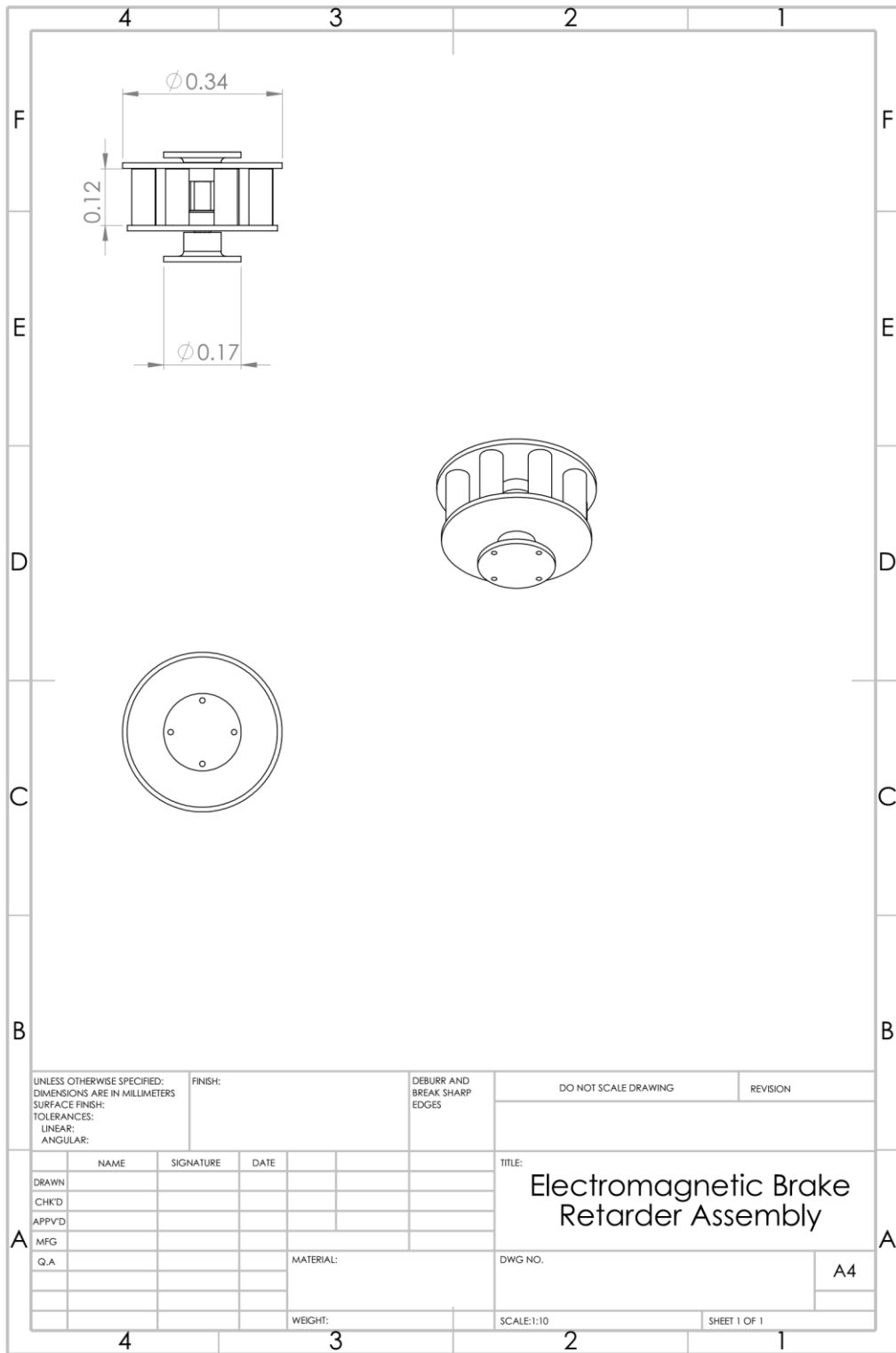
$$Module = \frac{pitch\ diameter}{Number\ of\ teeth} = \frac{30mm}{10} = 3mm$$

- **Addendum (a)** = It is the radial distance between a tooth's pitch circle and its top;
 $= 1 * module = 3mm$
- **Dedendum (b)**: The radial distance between a tooth's pitch circle and its bottom =
 $1.25 * module = 1.25 * 3mm = 3.75mm$
- **Clearance** = The radial distance between top and bottom teeth in a meshing gear. Clearance circle is a circle that passes through the top of the connected gear =
 $0.157 * module = 0.157 * 3mm = 0.471mm$
- **working depth** = It represents the radial distance between the addendum circle and the clearing circle. It is equivalent to the sum of the two meshing gears' addition =
 $2.25 * module = 2.25 * 3mm = 6.75mm$

4	3	2	1
F			F
E			E
D			D
C			C
B			B
UNLESS OTHERWISE SPECIFIED: DIMENSIONS ARE IN MILLIMETERS		FINISH:	DEBURR AND BREAK SHARP EDGES
SURFACE FINISH: TOLERANCES: LINEAR: ANGULAR:		DO NOT SCALE DRAWING	
		REVISION	
DRAWN	NAME	SIGNATURE	DATE
CHK'D			
APP'VD			
MFG			
Q.A			
		MATERIAL:	DWG NO.
			A4
		WEIGHT:	SCALE:1:5
			SHEET 1 OF 1
4	3	2	1
A			A







UNLESS OTHERWISE SPECIFIED: DIMENSIONS ARE IN MILLIMETERS		FINISH:		DEBURR AND BREAK SHARP EDGES		DO NOT SCALE DRAWING		REVISION	
SURFACE FINISH:									
TOLERANCES:									
LINEAR:									
ANGULAR:									
DRAWN		NAME	SIGNATURE	DATE	TITLE: Electromagnetic Brake Retarder Assembly				
CHK'D									
APP'VD									
MFG									
Q.A					MATERIAL:		DWG NO.		A4
					WEIGHT:		SCALE:1:10		SHEET 1 OF 1

APPENDIX 5: MATLAB SCRIPT FOR PLOTTING

The following MATLAB script was used to plot magnetic flux vs number of turns, magnetic flux density vs current, magnetic flux density vs air gap, magnetic flux density vs braking torque and current vs braking torque relation.

```
>> % Given Parameters
```

```
t_disc = 0.012; % Thickness of the rotating disc (m)
```

```
m_vehicle = 25000; % Total mass of vehicle (kg)
```

```
r_disc = 0.170; % Radius of rotating disc (m)
```

```
A_disc = 0.09079; % Area of rotating disc (m2)
```

```
J_e = 63207232.2; % Current density (A/m2)
```

```
omega = 167.55; % Angular velocity (rad/s)
```

```
Roho = 4.066e-8; % Material Resistivity (ohm-m)
```

```
N_range = 800:1:1000; % Number of turns
```

```
l_g_range = 0.0009:0.0001:0.0015; % Air gap (m)
```

```
mu = 1.256e-6; % Permeability of free space (N/A2)
```

```
sigma = 2.459e7; % Material conductivity (Siemens/m)
```

```
a_d = 0.135; % Distance between center of the disc to pole face
```

```
r_p = 0.025; % Radius of pole face
```

```
i_range = 10:1:19; % Current (A)
```

```
i_fixed = 19; % Fixed current (A)
```

```
N_fixed = 900; % Fixed number of turns
```

```
lg_fixed = 0.0012; % Fixed air gap (m)
```

```
% 1. Magnetic Flux Density (B) vs Number of Turns (N)
```

```
figure;
```

```
B_N = arrayfun(@(N) (N * i_fixed) / ((lg_fixed/mu) + (sigma * a_d * r_p * t_disc * omega)),  
N_range);
```

```
plot(N_range, B_N);
```

```

xlabel('Number of Turns (N)');
ylabel('Magnetic Flux Density (B) (T)');
title('Magnetic Flux Density vs Number of Turns');
grid on;

```

```

% 2. Magnetic Flux Density (B) vs Current (i)

```

```

figure;
B_i = arrayfun(@(i) (N_fixed * i) / ((l_g_fixed/mu) + (sigma * a_d * r_p * t_disc * omega)),
i_range);
plot(i_range, B_i);
xlabel('Current (i) (A)');
ylabel('Magnetic Flux Density (B) (T)');
title('Magnetic Flux Density vs Current');
grid on;

```

```

% 3. Magnetic Flux Density (B) vs Air Gap (l_g)

```

```

figure;
B_lg = arrayfun(@(l_g) (N_fixed * i_fixed) / ((l_g/mu) + (sigma * a_d * r_p * t_disc * omega)),
l_g_range);
plot(l_g_range, B_lg);
xlabel('Air Gap (m)');
ylabel('Magnetic Flux Density (B) (T)');
title('Magnetic Flux Density vs Air Gap');
grid on;

```

```

% 4. Magnetic Flux Density (B) vs Braking Torque (T_b)

```

```

figure;
T_b_range = arrayfun(@(i) ...

```

```
(Roho * (sigma * a_d * omega * (N_fixed * i) / ((lg_fixed/mu) + (sigma * a_d * r_p * t_disc * omega)))^2 * A_disc * t_disc) / omega, i_range);
```

```
B_Tb = arrayfun(@(Tb) (N_fixed * Tb) / ((lg_fixed/mu) + (sigma * a_d * r_p * t_disc * omega)), T_b_range);
```

```
plot(T_b_range, B_Tb);
```

```
xlabel('Braking Torque (T_b) (Nm)');
```

```
ylabel('Magnetic Flux Density (B) (T)');
```

```
title('Magnetic Flux Density vs Braking Torque');
```

```
grid on;
```

```
% 5. Current (i) vs Braking Torque (T_b)
```

```
figure;
```

```
T_b = arrayfun(@(i) ...
```

```
(Roho * (sigma * a_d * omega * (N_fixed * i) / ((lg_fixed/mu) + (sigma * a_d * r_p * t_disc * omega)))^2 * A_disc * t_disc) / omega, i_range);
```

```
plot(i_range, T_b);
```

```
xlabel('Current (i) (A)');
```

```
ylabel('Braking Torque (T_b) (Nm)');
```

```
title('Current vs Braking Torque');
```

```
grid on;
```